HHS Public Access

Author manuscript

Exp Hematol. Author manuscript; available in PMC 2024 July 06.

Published in final edited form as:

Exp Hematol. 2023 December ; 128: 48–66. doi:10.1016/j.exphem.2023.08.005.

Complementary and countervailing actions of Jak2 and Ikk2 in hematopoiesis in mice

Daniel A.C. Fisher,
Angelo B.A. Laranjeira[1],
Tim Kong,
Steven C. Snyder[2],
Kevin Shim,
Mary C. Fulbright,
Stephen T. Oh

Division of Hematology, Department of Medicine, Washington University School of Medicine, Saint Louis, MO

Abstract

Hyperactivation of JAK2 kinase is a unifying feature of human *Ph*— myeloproliferative neoplasms (MPNs), most commonly due to the *JAK2 V617F* mutation. Mice harboring a homologous mutation in the *Jak2* locus exhibit a phenotype resembling polycythemia vera. NFκB pathway hyperactivation is present in myeloid neoplasms, including MPNs, despite scarcity of mutations in NFκB pathway genes. To determine the impact of NFκB pathway hyperactivation in conjunction with Jak2 V617F, we utilized *Ikk2* (*Ikk2*-CA) mice. Pan-hematopoietic *Ikk2*-CA alone produced depletion of hematopoietic stem cells and B cells. When combined with the *Jak2 V617F* mutation, *Ikk2*-CA rescued the polycythemia vera phenotype of *Jak2 V617F*. Likewise, *Jak2 V617F* ameliorated defects in hematopoiesis produced by *Ikk2*-CA. Single-cell RNA sequencing of hematopoietic stem and progenitor cells revealed multiple genes antagonistically regulated by Jak2 and Ikk2, including subsets whose expression was altered by *Jak2 V617F* and/or *Ikk2*-CA but partly or fully rectified in the double mutant. We hypothesize that Jak2 promotes hematopoietic stem cell population self-renewal, whereas Ikk2 promotes myeloid lineage differentiation, and biases cell fates at several branch points in hematopoiesis. Jak2 and Ikk2 both regulate multiple

Address correspondence to Stephen T. Oh, Division of Hematology, Department of Medicine, Washington University School of Medicine, Saint Louis, MO, 63110.; stoh@wustl.edu.
[1]Present address: Incyte Corporation, Wilmington, Delaware.
[2]Present address: Abbvie, Dallas, Texas.

Author Contributions

Experiments detailing phenotypes of mice were performed by SCS and DACF, with assistance from MCF and ABAL. Bone marrow and HSC transplants were done by DACF and ABAL, with assistance from MCF. Mouse colony maintenance and genotyping were done by MCF. Sc-RNA-Seq analysis in Seurat was done by TK and KS, in consultation with DACF. Figures were prepared by DACF and TK, and text written by DACF and STO, with the contribution from other authors.

Conflict of Interest Disclosure

STO has served as a consultant for Kartos Therapeutics, CTI Bio-Pharma, Celgene/Bristol Myers Squibb, Disc Medicine, Blueprint Medicines, PharmaEssentia, Constellation, Geron, Abbvie, Sierra Oncology, and Incyte. DACF owns stock in Abbvie. Other authors declare no conflicts of interest.

SUPPLEMENTARY MATERIALS

Supplementary material associated with this article can be found in the online version at https://doi.org/10.1016/j.exphem.2023.08.005.

genes affecting myeloid maturation and cell death. Therefore, the presence of dual Jak2 and NF κB hyperactivation may present neomorphic therapeutic vulnerabilities in myeloid neoplasms.
Published by Elsevier Inc. on behalf of ISEH – Society for Hematology and Stem Cells.

Graphical Abstract

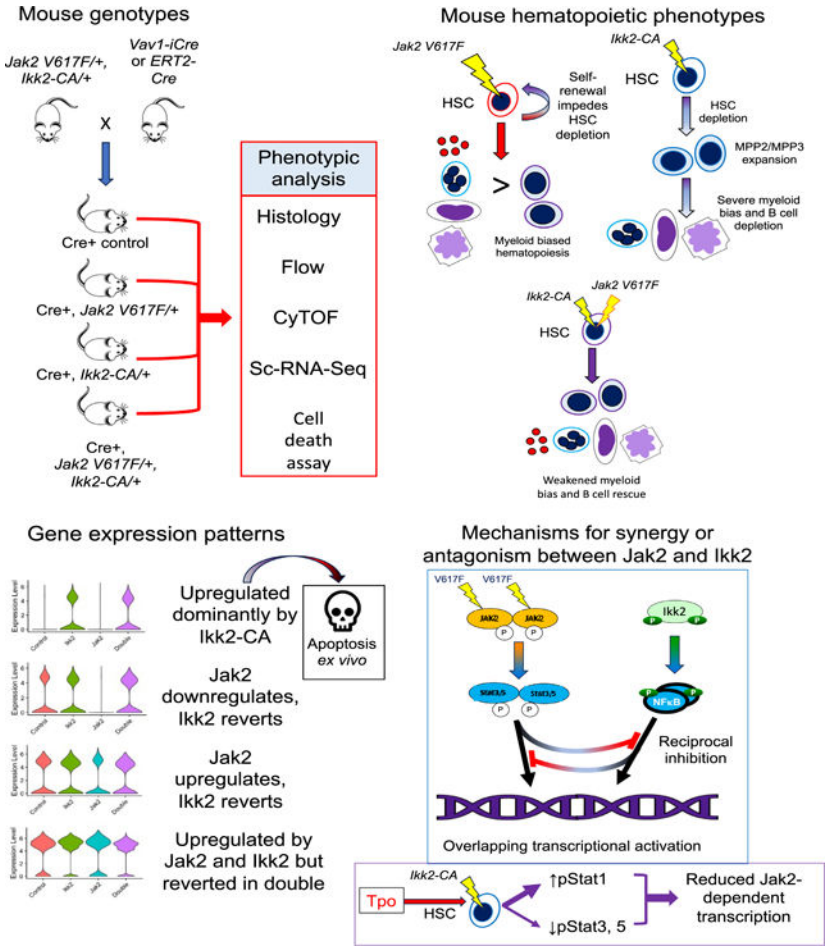

Hyperactivation of JAK2 kinase is a common feature among human *Ph*— myeloproliferative neoplasms (MPNs) [1], and has also been hypothesized as a defining feature of leukemic stem cells in acute myeloid leukemia (AML) [2]. Myeloid neoplasms have been found to harbor dysregulation of multiple intracellular signaling pathways, among which one of the most widespread is the NF κB signaling pathway. NF κB pathway hyperactivation has been identified in AML, myelodysplastic syndromes (MDS), chronic myeloid leukemia (CML), and MPNs [3–6]. The prevalence of NF κB pathway hyperactivation in each of these neoplasms, however, is not yet known. Furthermore, the etiology and consequences of NF κB pathway hyperactivation in myeloid neoplasms are not well understood. Mutations in genes intrinsic to NF κB signaling are very rare in myeloid neoplasms [7–9], therefore NF κB activation must be derived secondarily from a precedent pathophysiologic process. In MPNs, NF κB pathway hyperactivation has been hypothesized to derive from the secretion of activating ligands tumor necrosis factor (TNF), interleukin 1 (IL-1), or S100A8/A9,

from the malignant clone [5,10–12]. TNF, in addition to activating NFκB, also activates cell death signals [13]. It has been hypothesized that NFκB protects hematopoietic stem cells (HSCs) from TNF toxicity [14], and that this protection is active in preleukemic and leukemic stem cells in AML [15,16] and MPNs [10,17]. In a recent study, we found that inhibition of NFκB signaling with the pharmacologic inhibitor pevonedistat can ameliorate the phenotypes of Jak2 V617F and retroviral MPL W515L MPN mouse models, and reduce the expansion of human patient-derived MPN cells in xeno-grafted mice [18].

The purpose of the present study was to model NFκB pathway hyperactivation in mice in the context of an MPN, and to identify the potential contributions of NFκB pathway hyperactivation to the disease process. Among MPN mouse models, those expressing the activating *V617F* mutation in the endogenous mouse *Jak2* locus exhibited phenotypes resembling polycythemia vera or essential thrombocythemia [19–23]. Mice harboring pan-hematopoietic NFκB hyperactivation resulting from a synthetic activating mutation of the Iκ;kB kinase Ikk2 have also been described: these mice exhibited HSC depletion with enhanced proliferation of progenitor cells, and downregulation of genes associated with stemness and quiescence [24,25]. For the present study, this constitutive *Ikk2* allele has been crossed into mice expressing Jak2 V617F in the endogenous locus [20], to identify how NFκB hyperactivation can contribute to and alter an MPN phenotype in vivo. For purposes of this study, the constitutive Ikk2 kinase harboring mutations S177E and S181E is referred to as Ikk2-CA, and mice harboring a Cre-inducible cDNA encoding *Ikk2*-CA recombined into the ROSA26 locus, allele *R26StopFLikk2ca* [26], are referred to as Ikk2-CA mice, with the Cre-activated allele referred to as *Ikk2-CA*. Mice with a Cre-activated inducible allele of *Jak2 V617F* [20], recombined into the endogenous genomic locus, are termed Jak2 V617F mice, and the active allele is described as *Jak2 V617F.*

Results of the present study indicate that *Jak2 V617F* and *Ikk2*-CA have distinct, and sometimes opposing, effects in steady-state hematopoiesis, particularly in HSCs and early progenitors. We have observed that both mutations led to impairment of stem cell function, that *Ikk2*-CA altered the effects of thrombopoietin (Tpo) signaling by promoting phosphorylation of Stat1 over Stat3 and Stat5, that multiple genes whose expression was altered by both single mutations were partly rectified in the double mutant, and that *Ikk2*-CA produced a dominant propensity in LSK (Lin-Sca-1+Kit+ cells) and HSC to undergo apoptosis in ex vivo culture.

MATERIALS AND METHODS

Mice

Mouse strains were obtained from the following sources: Jak2 V617F from Ann Mullally (Dana-Farber Cancer Institute, Harvard), Ikk2-CA (*R26Stop*^{FL}*ikk2ca*) from Yousef Abu-Amer (Washington University), and Vav1-iCre (B6.Cg-Tg(Vav1-cre)A2Kio/J) and *cis*-NF-κB^{EGFP} (FVB.Cg-Tg(HIV-EGFP,luc)8Tsb/J) from Jackson Laboratory. Retroviral constructs for *MPL* W515L model [27] used as a positive control for fibrosis were obtained from Ross Levine. All procedures were conducted in accordance with the Institutional Animal Care and Use Committee of Washington University. Both male and female mice were used for all experiments, as no phenotypic differences by sex were observed. Visibly moribund mice

were not counted for parameters measured for live mice (Figures 1C–5) but were instead sacrificed and counted as mouse deaths (Figure 1A, B).

Antibodies

Antibodies for immunohistochemistry, flow cytometry, and mass cytometry, and reagents used for these procedures are shown in Supplementary Table E1.

Histology and Immunohistochemistry

Isolated hindlimb bones were fixed in 10% neutral buffered formalin overnight, decalcified by acid/EDTA protocol, embedded in paraffin and sectioned at 5-μm thickness. Immunohistochemistry utilized antigen retrieval in Tris–ethylenediaminetetraacetic acid pH9 (IHC Antigen retrieval solution, ThermoFisher) for 30 min at 96°C, blocked in 3% bovine serum albumin (BSA) in phosphate-buffered saline (PBS) for 1 hour, and stained with antibodies in 1.5% BSA in PBS overnight at 4°C. Images were obtained using Leica LAS-X software on a Leica DM-2500 microscope.

Flow Cytometry

Flow cytometry staining was done according to standard procedures. For analysis of bone marrow, bone marrow was syringe-flushed from femur and tibia of individual mice, erythrocytes were lysed, and remaining cells recovered and stained in PBS + 2% heat-inactivated fetal bovine serum (HIFBS) + 1 mM EDTA. For analysis of peripheral blood, blood was layered over 2% Dextran-500 in calcium-/magnesium-free Dulbecco's modified PBS (DPBS) + 0.5 M EDTA + 10 U/mL heparin. Erythrocytes were lysed and leukocytes recovered as for bone marrow. Data were recorded on an LSR Fortessa X-20 analyzer (BD Biosciences). For apoptosis assay, cells were incubated with PE-Annexin V (BD Biosciences) for 1 hour following antibody staining. Data were analyzed using FlowJo (TreeStar). Statistical analyses utilized GraphPad Prism.

Bone Marrow and HSC Transplants

Bone marrow was syringe-flushed from femur and tibia of individual mice. Leukocytes were recovered in DPBS + 0.5% BSA + 2 mM EDTA at 20 M cells/mL. Cd45.1 recipient mice were lethally irradiated (550 rads, two times separated by a 4- to 5-hour interval). For whole bone marrow transplants, 2 M donor cells total were injected into each recipient. For HSC transplants, Kit+ cells were purified using Cd117 microbead kit on AutoMACS separator (Miltenyi). Immunophenotypic HSC were sorted according to gating shown in Supplementary Figure E9. For HSC transplant, 250 HSC and 350,000 Cd45.1+ whole bone marrow cells were injected in 200 μL buffer into each recipient through the tail vein. For HSC Cd41— transplant, 200 Cd41— HSC and 350 thousand Cd45.1+ whole bone marrow cells were injected.

Colony-forming Assays

Kit+ cells were purified from bone marrow using a Cd117 microbead kit on an AutoMACS separator (Miltenyi). Kit+ cells were stained with antibody panel in Supplementary Table E1 and sorted on a MoFlo sorter (Beckman Coulter) according to gating in Supplementary

Figure E9A. Single HSCs were sorted into wells of 96-well plates previously seeded with irradiated (to prevent cell division) cells of the AFT 024 mouse bone marrow stroma−derived cell line. HSCs were cultured on lawns of AFT 024 cells for 2 weeks in cytokine-rich media: RPMI 1640 medium (ThermoFisher) supplemented with 5% heat-inactivated fetal bovine serum (HIFBS), 1% penicillin/streptomycin, 2 mM L-glutamine, 25 ng/mL each of Tpo, stem cell factor (Scf), FMS-like tyrosine kinase ligand (Flt3-L), and granulocyte colony−stimulating factor (Gcsf), and 10 ng/mL each of IL-3 and granulocyte/monocyte colony−stimulating factor (Gmcsf). Following the 2-week period, “cobblestone” colonies were counted (Supplementary Figure E2). Individual “cobblestone” colonies were resuspended, and divided into equal volumes for replating in cytokine-rich methocult M3434 (StemCell Technologies), with or without addition of 10 ng/mL Tnf. Tnf and other cytokines were from Peprotech. Following 2-week culture in methocult, CFU (colony-forming unit) colonies were counted, and tabulated as erythroid, myeloid, or blast like. Calculations to derive rates of CFU formation from HSC are described in the legend of Supplementary Figure E2.

Mass Cytometry

Mass cytometry was conducted on selected Kit+ selected cells from individual mice, as previously described. Protocol used was a variation on previously published human cell signaling CyTOF protocol [5,28]. Cells were labeled for viability with cisplatin [28,29] and incubated ex vivo in RPMI 1640 + 10% HIFBS + 1% penicillin/streptomycin, 2 mM L-glutamine for 1 hour, followed by stimulation with 50 ng/mL Tpo or Tnf (Peprotech), or unstimulated as control, for 15 min. Cells were immediately fixed in 1.6% formaldehyde by addition of an equal volume of 3.2% formaldehyde in PBS to cultures, for 10 min at room temperature. Fixed cells were stained with a panel of surface marker antibodies, followed by permeabilization in methanol at −20°C, resuspension, and staining with a panel of intracellular signaling antibodies (Supplementary Table E1). Stained cells were fixed, barcoded, and suspended in Irintercalator per protocol [28]. Data were recorded on a CyTOF2 mass cytometer (Fluidigm) and analyzed in Cytobank (cytobank.org).

Single-Cell RNA Sequencing

Bone marrow cells from five mice of each genotype were pooled, and Kit+ cells were purified using Cd117 microbead kit on AutoMACS separator (Miltenyi). Kit+ cells were stained with an antibody panel in Supplementary Table E1 and sorted on MoFlo sorter (Beckman Coulter) according to gating shown in Supplementary Figure E8A, B, E. Sorted LSK (Lin-Sca-1+Kit+) cells were resuspended at 1,000/μL density in 1 × PBS with 0.04% BSA. Cells were subjected to droplet bead capture, followed by cell lysis, reverse transcription, and amplification according to TotalSeqA protocol from 10X Genomics. Single-cell−derived cDNA libraries were sequenced on NovaSeq S4 cell sequencer (Illumina). CellRanger (10x Genomics, version 3.0.1) was used for transcript alignment, counting, and interlibrary normalization of single-cell samples. Aggr function was used to merge genotype libraries into a single data set, and initial visualization utilized Loupe-Browser version 6.0 (10X Genomics). Cluster and gene expression analysis utilized Seurat version 4.0.0 [30,31]. Cells with <500 or >7,500 genes captured per cell were removed from analysis, as were cells with 10% or more mitochondrial transcripts. RNA reads

were normalized with LogNormalize, and data were scaled. Unsupervised cell clustering was performed using an unanchored version of the uniform manifold approximation and projection (UMAP) algorithm in Seurat (number of cells per cluster in each genotype shown in Supplementary Table E2). Differential gene expression analysis between populations/samples of interest was performed utilizing FindAll-Markers with the Wilcoxon rank sum test. Gene set enrichment analysis of DEGs was run using fgsea [32] and the Hallmark gene set from msigdbr. Cell populations were identified from cluster expression of canonical HSC and progenitor population markers and NFκB target genes (Supplementary Table E3). Transcription factor analysis was done using DoRothEA (Bioconductor) in R.

Cell Culture for Apoptosis Assay

Kit+ selected cells from individual mice were purified using a Cd117 microbead kit on AutoMACS separator (Miltenyi). Cells were cultured for time intervals indicated in experiments, in cytokine-rich medium composed of RPMI 1640 medium (ThermoFisher) supplemented with 5% HIFBS, 1% penicillin/streptomycin, 2 mM L-glutamine, 25 ng/mL each of Tpo, Scf, Flt3-L, and Gcsf, and 10 ng/mL each of IL-3 and Gmcsf. All cytokines were obtained from Peprotech. For the zero-hour time point in time course experiments, cells were not cultured but immediately immunostained. Following the culture period, cells were resuspended in PBS + 2% HIFBS + 1 mM EDTA and immunostained with antibodies listed in Supplementary Table E1. Following immunostaining, cells were washed with DPBS and resuspended in Annexin V−binding buffer from PE Annexin VApoptosis Detection Kit I (BD Biosciences) and incubated with PE-Annexin V and 7-AAD from kit per manufacturer's protocol.

RESULTS

Jak2 V617F Rescues Survival in *Ikk2-CA* Mice

Mice harboring *Ikk2-CA* and *Jak2 V617F* alleles were crossed with *Vav1-iCre*-expressing transgenic mice, to obtain pan-hematopoietic expression of either or both activated kinase alleles beginning embryonically [33]. Parental mice were also crossed with mice expressing GFP under an NFκB-inducible promoter [34] to identify levels of chronic NFκB activity in mutant and control mice. *Ikk2-CA* and Jak2 *V617F* alleles were invariably heterozygous throughout experiments, avoiding confounding effects of gene dosage.

Mice expressing *Ikk2-CA* under control of *Vav1-iCre* have been reported previously, with homozygosity fatal in the first postnatal month [25] but without lethality in heterozygous mice [24]. In contrast, we observed progressive fatality among heterozygous Ikk2-CA mice, with median survival of 26 weeks postnatal (Figure 1A). Jak2 V617F mice also exhibited significantly greater fatality than controls (mice harboring Vav1-iCre allele alone), but median survival was not reached within 80 postnatal weeks. Double mutant Jak2 V617F, Ikk2-CA mice, however, exhibited mortality that was significantly greater than in controls but also significantly less than in Ikk2-CA mice, and not significantly different from Jak2 V617F mice. Therefore, *Jak2 V617F* rescued the mortality produced by *Ikk2-CA*, but *Ikk2-CA* did not rescue mortality related to *Jak2 V617F*.

Addition of antibiotics to water rescued the lethality of *Ikk2-CA.* With this treatment, only double mutant mice experienced inferior survival to single mutants and controls (Figure 1A). Based on the rescue and the identification of opportunistic infections in necropsies of untreated Ikk2-CA mice, their mortality is likely attributable to immunodeficiency. Notably, survival of Jak2 V617F mice also improved with antibiotic treatment. In contrast, when an inducible *ERT2-Cre* allele was used to induce *Ikk2-CA* and/or Jak2 *V617F* in mice cotransplanted with a 1:1 ratio of mutant or control donor bone marrow to wild-type competitor before induction with tamoxifen, both Jak2 V617F and double mutant mice showed significant mortality, indicating the presence of dominant disease produced by Jak2 *V617F,* which was not eliminated by *Ikk2-CA* (Figure 1B).

Ikk2-CA Opposes Myeloproliferative Phenotype Conferred by *Jak2 V617F*

Jak2 V617F mice, as previously described [20,35], exhibited a phenotype resembling polycythemia vera, featuring elevated counts of leukocytes, erythrocytes, and platelets (Figure 1C–F). In Ikk2-CA mice, these parameters typically fell below control values. Values of hematopoietic parameters in double mutant mice were intermediate between those from the single mutants, resembling those in control mice. Body weight, however, was depressed in double mutants as in Ikk2-CA (Supplementary Figure E4). Both Ikk2-CA and double mutants exhibited slight but significant splenic enlargement and evidence of splenic hematopoiesis, but neither exhibited the severe splenomegaly observed in Jak2 V617F mice (Figure 1D). Hence myeloproliferative disease produced by *Jak2 V617F* was partly but not completely rectified by addition of *Ikk2-CA*. Double mutants, as well as both single mutants, showed histologic evidence of neutrophils and abundant megakaryocytes in the spleen (Supplementary Figure E5). Double mutant bone marrows, as well as single mutant bone marrows, showed high cellularity, with evidence of both highly abundant neutrophils, as in Ikk2-CA, and megakaryocytes, as in Jak2 V617F mice (Supplementary Figure E7). All three mutant genotypes showed abnormal blood counts skewed toward neutrophils and monocytes, and away from lymphocytes (Figure 1G–L; Supplementary Figure E7).

Jak2 *V617F* and/or *Ikk2-CA* were induced with the use of *ERT2-Cre* and tamoxifen, in a competitive transplant, in which mutant or control (*ERT2-Cre* alone) Cd45.2+ bone marrow cells were transplanted at 1:1 ratio with Cd45.1+ wild-type competitor into lethally irradiated recipient mice (Figure 2). In these mice, a myeloproliferative phenotype was observed in recipients of both Jak2 V617F and double mutant bone marrow. Therefore, *Ikk2-CA* was insufficient to eliminate a myeloproliferative disease phenotype induced by *Jak2 V617F,* in the presence of wild-type bone marrow cells sufficient to rescue lethality of *Ikk2-CA* alone. *Jak2 V617F* and double mutant genotypes conferred a similar slight but significant competitive advantage over wild-type competitors, which was not observed with *Ikk2-CA* alone or control (Figure 9F, G).

Analysis of bone marrow showed no evidence of either myelofibrosis or leukemia in single or double mutant mice (Supplementary Figure E6). All three mutant genotypes showed hyperplasia of monocytic and megakaryocytic lineages; however, depletion of the B-cell lineage in both single mutants and of the T-cell lineage in Jak2 V617F mutants were not significantly evident in double mutant mice (Figure 3). Older Ikk2-CA mice

(≥27 weeks) exhibited severe depletion of the B-cell lineage (Figure 3G), consistent with immunodeficiency. This defect, as well as megakaryocytic hyperplasia (Figure 3D), and, in older mice, elevated proportions of myeloid, granulocytic, T, and LSK cells in Ikk2-CA bone marrow (Supplementary Figure E7), were partially rectified in double mutant mice.

Jak2 V617F and *Ikk2-CA* Exhibit Opposite Effects on HSC Prevalence but Combine to Impair HSC Engraftment

Bone marrow LSK cells were analyzed by flow cytometry to identify effects of the interaction of Jak2 *V617F* and *Ikk2-CA* on hematopoietic stem and progenitor (HSPC) cell populations (Figure 4, Supplementary Figure E3). As previously described [24], 8- to 20-week-old Ikk2-CA mice exhibited HSC depletion despite hyperabundance of LSK progenitor cells (Figure 4A–D). Ikk2-CA mice also exhibited contraction of the multipotent progenitor MPP1 population and expansion of MPP2 and MPP3, suggestive of accelerated myeloid lineage differentiation (Figure 4E–G). In double mutant mice, the depletion of HSC resembled that in Ikk2-CA mice. MPP2 expansion was observed in all mutant genotypes, whereas MPP3 expansion and MPP1 depletion were observed in Ikk2-CA and double mutant mice but not in Jak2 V617F mice. An NFκB-sensitive GFP reporter showed elevated chronic NFκB-dependent transcriptional activity induced by *Ikk2-CA*, with no effect of *Jak2 V617F* either alone or together with *Ikk2-CA*, in all HSPC populations (Figure 4I, J, Supplementary Figure E8).

Frequency of functional HSC was tested by competitive bone marrow transplantation. Whole bone marrow cells from mutant and control mice were cotransplanted with Cd45.1 competitor bone marrow cells at 1:1 and 9:1 ratios, respectively, into lethally irradiated Cd45.1 recipients. Cd45.2+ chimerism in recipient mice suggested a prevalence of functional HSCs of roughly one-fourth of control in Jak2 V617F mice, and lower still in Ikk2-CA and double mutant mice (Figure 5A; Supplementary Figures E1 and E9).E9 When equal numbers of immunophenotypic HSCs from each genotype were transplanted together with supporting Cd45.1 bone marrow cells as a competitor, functional impairment was revealed in immunophenotypic HSCs from either of the single mutant genotypes, with more severe impairment in double mutant HSCs (Figure 5B). Controlling for the presence of megakaryocyte-biased Cd41+ immunophenotypic HSCs, which are abundant but not transplantable in Jak2 V617F mice [36], all three mutant genotypes exhibited impaired HSC engraftment on a per-cell basis (Figure 5C). Bone marrow harvested 25 weeks posttransplant, however, showed that both Jak2 V617F and Ikk2-CA HSCs could produce long-term chimerism, whereas double mutant recipient mice invariably showed <10% bone marrow chimerism (Figure 5D, E). *Jak2 V617F* and *Ikk2-CA* combined to enhance monocyte fate in bone marrow, whereas opposing effects of *Jak2 V617F* and *Ikk2-CA* were observed on T cell presence in bone marrow and spleen, and granulocytes in the spleens of recipient mice (Supplementary Figure E2). In recipients of competitive transplants (at 1:1 ratio with wild-type Cd45.1+ bone marrow), in which mutant gene expression was induced with tamoxifen post-engraftment, the most salient finding was increased double mutant erythroid, granulocytic, and monocytic lineage cells in the spleen (Supplementary Figure E10). In colony-forming unit (CFU) assays, *Jak2 V617F* and *Ikk2-CA* both promoted myeloid colony formation at the expense of erythroid colonies, an effect that was maintained

in the double mutant, along with a significant reduction in overall colony formation from double mutant HSC versus those from any other genotype (Supplementary Figure E2).

Ikk2 Promotes Mitosis and Alters Tpo Signaling in HSCs

Mass cytometry (CyTOF) was utilized to assess intracellular signaling in Jak2 V617F, Ikk2-CA, and double mutant mice, as well as Vav1-iCre controls (Figure 6). Although the NFκB-responsive EGFP reporter demonstrated that Jak2 V617F did not substantially alter chronic NFκB signaling in HSPCs (Supplementary Figure E3)E8, the potential for interaction of downstream signaling was further assayed using antibodies to a panel of signaling molecules (Supplementary Table E1). Ikk2-CA and double mutant mice, but not Jak2 V617F mice, showed elevated labeling of the proliferation marker Ki67, among immunophenotypic HSCs (Figure 6A–C). They also showed an elevated proportion of pRela+IκBα— LSK and HSC, consistent with continuously active NFκB signaling (Figure 6D–F). In both HSC and overall LSK, proportions of basally pRela+IκBα— cells in Ikk2-CA and double mutant mice were observed in the range of 20%−50%, similar to proportions previously observed in HSPCs from human patients with myelofibrosis and secondary AML [5]. Notably, both *Ikk2-CA*-harboring genotypes showed lower levels of pStat3 and pStat5 induced by Tpo, compared with control and Jak2 V617F mice (Figure 6G–J; Supplementary Figures E11 and E12). In Ikk2-CA, but not double mutant mice, Tpo activated Stat1 phosphorylation more strongly than other genotypes, suggesting a shift in the balance of Stat1 versus Stat3 and Stat5 activation (Figure 6K). Single-cell RNA sequencing (Figures 7–9) identified a potential basis for this shift in gene expression: Ikk2-CA HSC and MPP expressed a higher level of *Stat1* mRNA than other genotypes, whereas it showed a reduced expression of *Stat3* (Figure 6L).

Jak2 and Ikk2 Promote Distinct Gene Expression Programs and Cell Fate Biases in HSC and Early Progenitors

Jak2 and Ikk2 kinases signal upstream from transcriptional factors of the Stat and NFκB families, respectively [37−39]. Therefore, we sought to identify the transcriptional programs produced in HSC and early hematopoietic progenitor cells by *Jak2 V617F* and *Ikk2-CA*, and by their combination in double mutant mice. Single-cell RNA sequencing was performed on pools of sorted LSK cells from five mice of each genotype. Greater transcript diversity per cell was detected in single mutants than in Vav1-iCre controls, and this was further elevated in double mutant cells, consistent with net activation of gene expression due to these mutations (Figure 7A, B). Cells numbering from >5,000 to >15,000 were identified in each sample, with >4,000 to >13,000 meeting feature thresholds (Figure 7C, Supplementary Figure E13). We utilized unbiased Seurat clustering [30,31] to generate a UMAP visualization with 21 clusters identifiable as distinct cell populations based on canonical HSPC subpopulation gene expression patterns and NFκB target gene expression (Figure 7D–H, Supplementary Tables E2 and E3). These included clusters for HSC and MPP, *Csf1r+* myelomonocytic progenitors, and cells with expression profiles of granulocyte/monocyte progenitors (GMP) and megakaryocyte/erythrocyte progenitors (MEP). A high expression of cell-cycle genes identified proliferating myeloid progenitors, in separate clusters from those with distinct gene expression patterns identified with HSC, GMP, MEP, or *Csf1r+* myelomonocytic progenitors. Separate clusters corresponding to each population

identified, were observed to be composed almost entirely of cells from Ikk2-CA and double mutants, rather than Jak2 V617F or Vav1-iCre, reflecting the strong effect of Ikk2-CA on transcription (Figure 7E, Supplementary Tables E2 and E3).

Ikk2-CA LSK cells showed amplification of a *Csf1r+* GMP-like subpopulation and of a population expressing B-cell genes, including immunoglobulin genes, which was only a minute component of LSK in the other three genotypes (Figure 7F, G, Supplementary Tables E2 and E3). The *Csf1r+* population was reduced by Jak2 *V617F* relative to control, and in double mutant relative to single *Ikk2-CA* mutant LSK. Cells expressing genes suggesting an MEP-like identity were amplified specifically in Jak2 *V617F* mutants. Although clusters identifiable as containing HSCs had only a very small representation in Ikk2-CA and double mutant LSK (clusters 1+3), consistent with the reduction in immunophenotypic HSC previously observed, a broader HSC + MPP grouping (1+3+4) was represented by more than 1,000 cells in each genotype (Figure 7F, G).

Transcription factor analysis of HSC clusters (1+3) showed multiple transcription factors to be more strongly expressed in Jak2 V617F and Ikk2-CA single mutants than in controls or double mutants, whereas the analysis of GMP groups (18+20+21, a subset of the broader *Csf1r+* population) grouped double mutants with Ikk2-CA, and Jak2 V617F mutants with controls (Figure 8A; Supplementary Figure E14; Supplementary Table E4). A gene set representing known Tnf/NFκB target genes was downregulated in double mutant HSC versus both Jak2 V617F and Ikk2-CA single mutants but not similarly downregulated in double mutant GMP (Figure 8B, C; Supplementary Table E5). This gene set was nonetheless more highly expressed in double mutant versus control HSC (NES 1.73; Padj = 0.073), but not to the extent observed in Ikk2-CA (NES 3.96; Padj = 0.0089), or Jak2 V617F (NES 3.48; Padj = 0.010) single mutants (Supplementary Table E5). This compares with NES values observed for NFκB-related gene sets in a range of 1.2−1.4, in a prior study of gene expression in human myelofibrosis patient versus normal CD34+ cells by microarray [5,40].

In the HSC + MPP cell population (1+3+4), gene expression patterns in both Jak2 V617F and Ikk2-CA single mutants differed substantially from control, with double mutant cells mainly clustering with those from Ikk2-CA (Figure 9A–C). Nonetheless, substantial differences were observed between the double mutant and either or both single mutants. Multiple genes were upregulated in both single mutants versus control but downregulated in double versus both single mutants (Figure 9D, Supplementary Figure E15, Supplementary Table E6). These included genes encoding transcription factors of the AP-1 family (*Fos, Jun, Fosb, Junb*), other transcription factors (*Klf2, Klf6, Egr1, Zfp36, Nr4a1, Nr4a2*), and signaling regulators (*Dusp1, Rgs1, Ier2, Ier5*). In the double mutant, genes encoding several NFκB signaling effectors and inflammatory cytokines nonetheless remained upregulated versus control (Figure 9E). Genes related to cell death showed differential expression, with apoptotic effectors *Ripk1, Bad, Bid, Casp1*, and *Casp4* being dominantly upregulated by *Ikk2-CA* (Figure 9F, Supplementary Figure E16).

Ikk2-CA Confers Dominant Ex Vivo Apoptotic Vulnerability

Because dual hyperactivation of both JAK2/STAT3,5 and NFκB pathway signaling is present in stem and progenitor cells of human myeloid neoplasm patients [5], and

because multiple apoptosis-related genes showed differential expression in the HSC + MPP cell population, we hypothesized that *Jak2 V617F* and *Ikk2-CA* would alter these cells' propensity for apoptosis. Although multiple apoptosis-related genes showed altered expression, these did not consistently predict either greater or lesser propensity to apoptosis in any mutant genotype (Supplementary Figure E16). Cleaved caspase 3 staining of bone marrow sections revealed both individual cells and cell clusters in all four genotypes, without any readily apparent difference. Selected Kit+ cells ex vivo showed no baseline difference in apoptosis in LSK or HSC populations, but after 48-hour culture in cytokine-rich medium [14], these cells from Ikk2-CA and double mutants became spontaneously apoptotic (Figure 10A–D; Supplementary Figure E17). In common myeloid progenitors (CMP), the greatest tendency to apoptosis ex vivo was observed in double mutant cells, whereas in GMP, spontaneous apoptosis was minimal. This suggested that *Ikk2-CA*, with or without *Jak2 V617F*, could confer greater susceptibility to an apoptogenic insult to HSC and early progenitors. In 24-hour culture, however, only Jak2 mutant cells showed significant apoptosis in response to Tnf, with apoptosis observed even without Tnf in Ikk2-CA and double mutant HSC (Supplementary Figure E17). Dose−response experiments with proapoptotic agents in 24-hour culture showed that HSC from all four genotypes were susceptible to apoptosis induced by LCL-161 but showed little to no susceptibility to navitoclax or venetoclax, although the latter produced apoptosis of CMP, which was more robust in all three mutants than in Vav1-iCre controls (Figure 10E, F). In CMP, GMP, and MEP, but not HSC or MPP, differential sensitivity to LCL-161 was observed (Supplementary Figure E18).

DISCUSSION

JAK2 is constitutively activated in MPNs and is associated with stem cell identity in AML [2]. The *JAK2 V617F* mutation is present in a majority of MPN patients, but its presence long predates evident disease [41], and it is found in cases of benign clonal hematopoiesis as well [42]. Although the presence of *Jak2 V617F* in mice confers a polycythemia vera-like phenotype, human neoplastic disease may require additional pathogenic factors. We have previously identified dysregulation of multiple signaling pathways in MPNs, including NFκB [5,18,43]. We utilized Ikk2-CA mice to model the potential effects of pan-hematopoietic NFκB hyperactivity in both absence and presence of Jak2 V617F. An important limitation of this approach is that *Ikk2-CA* is a synthetic constitutively active allele, and consequently it may produce NFκB activity much greater than exists in human patients. It is not fully comparable to *Jak2 V617F*, which replicates a human disease mutation. We and others have provided evidence that NFκB hyperactivity in MPN patients is likely secondary to chronic activity of JAK2 and/or the upstream kinase MPL [5,44].

Ikk2-CA mice have been published, both as homozygotes and heterozygotes, and were found to harbor a phenotype of HSC depletion [24,25]. Because hematopoietic homozygosity of *Ikk2-CA* was lethal [25] and excessive for our purpose, we used this mutation only in its heterozygous state. This proved progressively fatal to mice in the absence of prophylactic antibiotic treatment, suggesting immunodeficiency. The substantial depletion of B cells in Ikk2-CA mice, as well as the failure of Ikk2-CAT cells to colonize the spleen, suggests multiple immune defects, which were not the focus of our study. The

rescue of double mutant mice from the untreated Ikk2-CA lethality, however, suggested a previously undescribed opposition between Jak2 and Ikk2. The amelioration of the Jak2 V617F myeloproliferative phenotype in double mutant mice suggested the same. Variable phenotypes among mice of the same genotype could be due in part to incomplete excision of floxed alleles, based on variable *Cre* expression, as has been reported for ERT2-Cre [45]. Alternatively, they may simply result from random dynamic variation in progressively developing phenotypes, which we have observed in all mutant genotypes. Despite the *Ikk2-CA* mutation being synthetic and therefore nonphysiological, the fact that its resulting phenotype was partly rescued by the physiologic *Jak2 V617F* mutation suggests that the interactions between the effects of these mutations, as described in our study, could plausibly be operant in human myeloid neoplasms. To the extent that metrics of NFκB pathway activity observed in our study are comparable to those in prior studies on human patient samples (in percentages of cells with NFκB activity detectable by CyTOF, and magnitude of gene expression changes vs. control), the effects induced by Ikk2-CA appeared similar to or greater than those in human patients but not by multiple orders of magnitude. Any such comparison available, however, likely underestimates the effects of continuous NFκB activity produced by Ikk2-CA, because physiologic NFκB activity is regulated temporally via negative feedback loops, which produce multiple patterns of periodicity in the expression of NFκB target genes [46]. The complexity of NFκB pathways, coupled with their temporal variability, makes any absolute quantitation of NFκB hyperactivation impossible. Indeed, evidence that “canonical” and “noncanonical” NFκB pathways can antagonize one another [47], implies that any generalized description of NFκB signaling in toto is likely to be oversimplified compared with the complex interplay of signaling effectors within a cell.

At first glance the interaction between *Jak2 V617F* and *Ikk2-CA* appears epistatic: *Jak2 V617F* causes myeloproliferation and *Ikk2-CA* produces leukopenia, and in this respect their effects largely cancel each other, although both produce a myeloid bias to hematopoiesis, which is therefore not reverted in the double mutant. Evidence that the NFκB-dependent GFP reporter was not diminished in double versus single Ikk2-CA mutants (Figure 2J, K; Supplementary Figure E8), suggests that Jak2 does not directly inhibit NFκB.

The addition of *Ikk2-CA* did not overtly change the Jak2 V617F phenotype to a different disease phenotype and did not abrogate Jak2 mutation effects altogether, suggesting that the double mutant phenotype was not entirely due to NFκB-dependent feedback inhibition of Jak2 (although this may be a partial explanation). One possible contribution to apparent Jak2 antagonism by Ikk2-CA is elevated expression of *Stat1* and reduced expression of *Stat3,* leading to greater activating phosphorylation of Stat1 by Tpo and reduced activation of Stat3 and Stat5 (Figure 6, Supplementary Figure E11). The evidence from sc-RNA-Seq that multiple genes are either upregulated or downregulated by both *Jak2 V617F* and *Ikk2-CA* but are reverted to or near control levels in double mutant cells, means that reciprocal signaling inhibition leads to reciprocal inhibition of effects on many (but not all) mutual transcriptional targets of Jak2 and Ikk2. This reciprocal signaling inhibition may, however, be dose dependent: In *Abi1* null mice, which have combined hyperactivation of Jak2 and NFκB signaling, the effects of these two pathways appear to complement more than oppose each other, as loss of *Abi1* was shown to exacerbate, rather than ameliorate, the

Jak2-activating MPL W515L retroviral mouse model phenotype [48]. Additionally, other factors differentially expressed among cell populations must regulate the valence of the interaction, as mutual antagonism was much less evident in GMP than in HSC or MPP.

Notably, substantial features of the phenotypes produced by all three mutant genotypes studied may develop non-cell-autonomously. For example, all three mutant genotypes sustain amplification of the MPP2 and MPP3 populations (Figure 3). A subpopulation of MPP3 has been observed to develop a secretory phenotype, which can contribute to leukemic or regenerative pathophysiology [49–51]. Likewise, monocytes, expanded by both *Jak2 V617F* and *Ikk2-CA*, are the primary cytokine-secreting cells in myelofibrosis [43], and granulocytes can also have an important role in secreting the NFκB-activating cytokine Tnf [49,52], which is relevant to AML and CML, as well as MPNs [10,15,53].

The evidence presented here suggests that strong NFκB activation may be more deleterious for hematopoiesis in the absence of Jak2 V617F than in its presence. This may be reflected by evidence for NFκB hyperactivation in myelodysplastic syndromes [4]. Substantial evidence supports the hypothesis that in MPNs, NFκB hyperactivation can be transmitted non-cell-autonomously from malignant cells to nonmalignant cells [5,11,44,52,54,55]. This is a potential mechanism for clonal dominance in MPNs [10] Further study is likely to be required to determine to what extent synergy versus antagonism of JAK-STAT and NFκB pathways are operant in JAK2-activated MPNs or other neoplasms.

Finally, *Ikk2-CA* made cultured LSK, and particularly HSC, undergo apoptosis spontaneously ex vivo, without any exogenously applied apoptogenic agent. This effect was intact in the presence of *Jak2 V617F,* and enhanced in double mutant CMP. Therefore, we hypothesize that NFκB hyperactivation predisposes malignant HSC and early progenitors to susceptibility to proapoptotic therapy. This hypothesis warrants further investigation in future studies.

Supplementary Material

Refer to Web version on PubMed Central for supplementary material.

Acknowledgments

We thank Roderick Lin and Ishita Gupta for assistance with mouse cell collection, Isadore Barton for mouse facility maintenance, and staff of Siteman Cancer Center flow cytometry core, Washington University, for assistance with cell sorting. We also thank Dr. Grant Challen for invaluable advice and assistance regarding HSC transplant and sc-RNA-Seq. We thank Olga N. Malkova, Dr. Diane Bender, and staff of the Immunomonitoring Laboratory at Washington University for technical assistance with mass cytometry and flow cytometry equipment. We thank Kevin Haub and Jennifer Ponce (Genome Technology Access Center, Washington University), for sc-RNA-Seq library preparation and sequencing. We thank Crystal Idleburg, Musculoskeletal Research Core, Washington University, for assistance with bone marrow histology. We thank Dr. Yousef Abu-Amer for advice regarding Ikk2-CA mice. We thank Fan He for introduction to DoRothEA.

Funding Sources

S.T. Oh has received a grant support from US National Institutes of Health (NIH) (Grants K08HL106576 and R01HL134952), a Challenge Grant from the MPN Research Foundation, Leukemia and Lymphoma Society Translational Research Program, and When Everyone Survives Foundation. T. Kong has received Canadian Institutes of Health Research Doctoral Foreign Study Award. Technical support was provided by the Alvin J. Siteman Cancer Center Flow Cytometry Core, and Immunomonitoring Laboratory, which are supported by US

National Cancer Institute (NCI) Cancer Center Support Grant P30CA91842. The Immunomonitoring Laboratory is also supported by the Andrew M. and Jane M. Bursky Center for Human Immunology and Immunotherapy Programs.

REFERENCES

1. Spivak JL. Myeloproliferative neoplasms. N Engl J Med 2017;376:2168–81. 10.1056/NEJMra1406186. [PubMed: 28564565]
2. Levine JH, Simonds EF, Bendall SC, et al. Data-driven phenotypic dissection of AML reveals progenitor-like cells that correlate with prognosis. Cell 2015;162:184–97. 10.1016/j.cell.2015.05.047. [PubMed: 26095251]
3. Guzman ML, Neering SJ, Upchurch D, et al. Nuclear factor-kappaB is constitutively activated in primitive human acute myelogenous leukemia cells. Blood 2001;98:2301–7. 10.1182/blood.v98.8.2301. [PubMed: 11588023]
4. Grosjean-Raillard J, Tailler M, Ades L, et al. ATM mediates constitutive NF-kappaB activation in high-risk myelodysplastic syndrome and acute myeloid leukemia. Oncogene 2009;28:1099–109. 10.1038/onc.2008.457. [PubMed: 19079347]
5. Fisher DAC, Malkova O, Engle EK, et al. Mass cytometry analysis reveals hyperactive NF Kappa B signaling in myelofibrosis and secondary acute myeloid leukemia. Leukemia 2017;31:1962–74. 10.1038/leu.2016.377. [PubMed: 28008177]
6. Hsieh MY, Van Etten RA. IKK-dependent activation of NF-kB contributes to myeloid and lymphoid leukemogenesis by BCR-ABL1. Blood 2014;123:2401–11. 10.1182/blood-2014-01-547943. [PubMed: 24464015]
7. Ley TJ, Miller C, Ding L, et al. Genomic and epigenomic landscapes of adult de novo acute myeloid leukemia. N Engl J Med 2013;368:2059–74. 10.1056/NEJMoa1301689. [PubMed: 23634996]
8. Miller CA, Wilson RK, Ley TJ. Genomic landscapes and clonality of de novo AML. N Engl J Med 2013;369:1473.. 10.1056/NEJMc1308782. 10 10.
9. Burd A, Levine RL, Ruppert AS, et al. Precision medicine treatment in acute myeloid leukemia using prospective genomic profiling: feasibility and preliminary efficacy of the beat AML master trial. Nat Med 2020;26:1852–8. 10.1038/s41591-020-1089-8. [PubMed: 33106665]
10. Fleischman AG, Aichberger KJ, Luty SB, et al. TNFalpha facilitates clonal expansion of JAK2V617F positive cells in myeloproliferative neoplasms. Blood 2011;118:6392–8. 10.1182/blood-2011-04-348144. [PubMed: 21860020]
11. Arranz L, Sanchez-Aguilera A, Martin-Perez D, et al. Neuropathy of haematopoietic stem cell niche is essential for myeloproliferative neoplasms. Nature 2014;512:78–81. 10.1038/nature13383. [PubMed: 25043017]
12. Laouedj M, Tardif MR, Gil L, et al. S100A9 induces differentiation of acute myeloid leukemia cells through TLR4. Blood 2017;129:1980–20. 10.1182/blood-2016-09-738005. [PubMed: 28137827]
13. Cabal-Hierro L, Lazo PS. Signal transduction by tumor necrosis factor receptors. Cell Signal 2012;24:1297–305. 10.1016/j.cell-sig.2012.02.006. [PubMed: 22374304]
14. Yamashita M, Passegué E. TNF-α coordinates hematopoietic stem cell survival and myeloid regeneration. Cell Stem Cell 2019;25:357–72.e7. 10.1016/j.stem.2019.05.019.. [PubMed: 31230859]
15. Kagoya Y, Yoshimi A, Kataoka K, et al. Positive feedback between NF-kappaB and TNF-alpha promotes leukemia-initiating cell capacity. J Clin Invest 2014;124:528–42. 10.1172/jci68101. [PubMed: 24382349]
16. Volk A, Li J, Xin J, et al. Co-inhibition of NF-kappaB and JNK is synergistic in TNF-expressing human AML. J Exp Med 2014;211:1093–108. 10.1084/jem.20130990. [PubMed: 24842373]
17. Heaton WL, Senina AV, Pomicter AD, et al. Autocrine Tnf signaling favors malignant cells in myelofibrosis in a Tnfr2-dependent fashion. Leukemia 2018;32:2399–411. 10.1038/s41375-018-0131-z. [PubMed: 29749399]

18. Kong T, Laranjeira ABA, Collins TB, et al. Pevonedistat targets malignant cells in myeloproliferative neoplasms in vitro and in vivo via NFκB pathway inhibition. Blood Adv 2022;6:611–23. 10.1182/bloodadvances.2020002804. [PubMed: 34644371]
19. Mullally A, Lane SW, Brumme K, Ebert BL. Myeloproliferative neoplasm animal models. Hematol Oncol Clin North Am 2012;26:1065–81. 10.1016/j.hoc.2012.07.007. [PubMed: 23009938]
20. Mullally A, Lane SW, Ball B, et al. Physiological Jak2V617F expression causes a lethal myeloproliferative neoplasm with differential effects on hematopoietic stem and progenitor cells. Cancer Cell 2010;17:584–96. 10.1016/j.ccr.2010.05.015. [PubMed: 20541703]
21. Li J, Spensberger D, Ahn JS, et al. JAK2 V617F impairs hematopoietic stem cell function in a conditional knock-in mouse model of JAK2 V617F-positive essential thrombocythemia. Blood 2010;116:1528–38. 10.1182/blood-2009-12-259747. [PubMed: 20489053]
22. Li J, Kent DG, Chen E, Green AR. Mouse models of myeloproliferative neoplasms: JAK of all grades. Dis Model Mech 2011;4:311–7. 10.1242/dmm.006817. [PubMed: 21558064]
23. Akada H, Akada S, Hutchison RE, Mohi G. Loss of wild-type Jak2 allele enhances myeloid cell expansion and accelerates myelofibrosis in Jak2V617F knock-in mice. Leukemia 2014;28:1627–35. 10.1038/leu.2014.52. [PubMed: 24480985]
24. Nakagawa MM, Chen H, Rathinam CV. Constitutive activation of NF-kB pathway in hematopoietic stem cells causes loss of quiescence and deregulated transcription factor networks. Front Cell Dev Biol 2018;6:143. 10.3389/fcell.2018.00143. [PubMed: 30425986]
25. Nakagawa MM, Rathinam CV. Constitutiveactivation of the canonical NF-κB pathway leads to bone marrow failure and induction of erythroid signature in hematopoietic stem cells. Cell Rep 2018;25:2094–109.e4. 10.1016/j.celrep.2018.10.071.. [PubMed: 30463008]
26. Sasaki Y, Derudder E, Hobeika E, et al. Canonical NF-kappaB activity, dispensable for B cell development, replaces BAFF-receptor signals and promotes B cell proliferation upon activation. Immunity 2006;24:729–39. 10.1016/j.immuni.2006.04.005. [PubMed: 16782029]
27. Pikman Y, Lee BH, Mercher T, et al. MPLW515L is a novel somatic activating mutation in myelofibrosis with myeloid metaplasia. PLoS Med 2006;3:e270. 10.1371/journal.pmed.0030270. [PubMed: 16834459]
28. Bandyopadhyay S, Fisher DAC, Malkova O, Oh ST. Analysis of signaling networks at the single-cell level using mass cytometry. Methods Mol Biol 2017;1636:371–92. 10.1007/978-1-4939-7154-1_24. [PubMed: 28730492]
29. Fienberg HG, Simonds EF, Fantl WJ, Nolan GP, Bodenmiller B. A platinum-based covalent viability reagent for single-cell mass cytometry. Cytometry A 2012;81:467–75. 10.1002/cyto.a.22067. [PubMed: 22577098]
30. Butler A, Hoffman P, Smibert P, Papalexi E, Satija R. Integrating single-cell transcriptomic data across different conditions, technologies, and species. Nat Biotechnol 2018;36:411–20. 10.1038/nbt.4096. [PubMed: 29608179]
31. Satija R, Farrell JA, Gennert D, Schier AF, Regev A. Spatial reconstruction of single-cell gene expression data. Nat Biotechnol 2015;33:495–502. 10.1038/nbt.3122. [PubMed: 25867923]
32. Korotkevich G, Sukhov V, Budin N, Shpak B, Artyomov MN, Sergushichev A. Fast gene set enrichment analysis. bioRxiv 2021:060012. 10.1101/060012.
33. Almarza E, Segovia JC, Guenechea G, Gómez SG, Ramírez A, Bueren JA. Regulatory elements of the vav gene drive transgene expression in hematopoietic stem cells from adult mice. Exp Hematol 2004;32:360–4. 10.1016/j.exphem.2004.01.005. [PubMed: 15050746]
34. Magness ST, Jijon H, Van Houten Fisher N, Sharpless NE, Brenner DA, Jobin C. In vivo pattern of lipopolysaccharide and anti-CD3-induced NF-kappa B activation using a novel gene-targeted enhanced GFP reporter gene mouse. J Immunol 2004;173:1561–70. 10.4049/jimmunol.173.3.1561. [PubMed: 15265883]
35. Mullally A, Poveromo L, Schneider RK, Al-Shahrour F, Lane SW, Ebert BL. Distinct roles for long-term hematopoietic stem cells and erythroid precursor cells in a murine model of Jak2V617F-mediated polycythemia vera. Blood 2012;120:166–72. 10.1182/blood-2012-01-402396. [PubMed: 22627765]

36. Rao TN, Hansen N, Stetka J, et al. JAK2-V617F and interferon-a induce megakaryocyte-biased stem cells characterized by decreased long-term functionality. Blood 2021;137:2139–51. 10.1182/blood.2020005563. [PubMed: 33667305]
37. Mulero MC, Wang VY, Huxford, Ghosh G. Genome reading by the NF-κB transcription factors. Nucleic Acids Res 2019;47:9967–89. 10.1093/nar/gkz739. [PubMed: 31501881]
38. Kleppe M, Kwak M, Koppikar P, et al. JAK-STAT pathway activation in malignant and nonmalignant cells contributes to MPN pathogenesis and therapeutic response. Cancer Discov 2015;5:316–31. 10.1158/2159-8290.CD-14-0736. [PubMed: 25572172]
39. Wilmes S, Hafer M, Vuorio J, et al. Mechanism of homodimeric cytokine receptor activation and dysregulation by oncogenic mutations. Science 2020;367:643–52. 10.1126/science.aaw3242. [PubMed: 32029621]
40. Norfo R, Zini R, Pennucci V, et al. miRNA-mRNA integrative analysis in primary myelofibrosis CD34+ cells: role of miR-155/JARID2 axis in abnormal megakaryopoiesis. Blood 2014;124:e21–32. 10.1182/blood-2013-12-544197. [PubMed: 25097177]
41. Williams N, Lee J, Mitchell E, et al. Life histories of myeloproliferative neoplasms inferred from phylogenies. Nature 2022;602:162–8. 10.1038/s41586-021-04312-6. [PubMed: 35058638]
42. Xie M, Lu C, Wang J, et al. Age-related mutations associated with clonal hematopoietic expansion and malignancies. Nat Med 2014;20:1472–8. 10.1038/nm.3733. [PubMed: 25326804]
43. Fisher DAC, Miner CA, Engle EK, et al. Cytokine production in myelofibrosis exhibits differential responsiveness to JAK-STAT, MAP kinase, and NFκB signaling. Leukemia 2019;33:1978–95. 10.1038/s41375-019-0379-y. [PubMed: 30718771]
44. Kleppe M, Koche R, Zou L, et al. Dual targeting of oncogenic activation and inflammatory signaling increases therapeutic efficacy in myeloproliferative neoplasms. Cancer Cell 2017;33:29–43.e7. 10.1016/j.ccell.2017.11.009.. [PubMed: 29249691]
45. Sandlesh P, Juang T, Safina A, Higgins MJ, Gurova KV. Uncovering the fine print of the CreERT2-LoxP system while generating a conditional knockout mouse model of Ssrp1 gene. PLoS One 2018;13:e0199785. 10.1371/journal.pone.0199785.
46. Gross S, Piwnica-Worms D. Real-time imaging of ligand-induced IKK activation in intact cells and in living mice. Nat Methods 2005;2:607–14. 10.1038/nmeth779. [PubMed: 16094386]
47. Jacque E, Tchenio T, Piton G, Romeo PH, Baud V. RelA repression of RelB activity induces selective gene activation downstream of TNF receptors. Proc Natl Acad Sci U S A 2005;102:14635–40. 10.1073/pnas.0507342102. [PubMed: 16192349]
48. Chorzalska A, Morgan J, Ahsan N, et al. Bone marrow-specific loss of ABI1 induces myeloproliferative neoplasm with features resembling human myelofibrosis. Blood 2018;132:2053–66. 10.1182/blood-2018-05-848408. [PubMed: 30213875]
49. Hérault A, Binnewies M, Leong S, et al. Myeloid progenitor cluster formation drives emergency and leukaemic myelopoiesis. Nature 2017;544:53–8. 10.1038/nature21693. [PubMed: 28355185]
50. Kang YA, Pietras EM, Passegué E. Deregulated Notch and Wnt signaling activates early-stage myeloid regeneration pathways in leukemia. J Exp Med 2020;217:e20190787. 10.1084/jem.20120787.
51. Pietras EM, Reynaud D, Kang YA, et al. Functionally distinct subsets of lineage-biased multipotent progenitors control blood production in normal and regenerative conditions. Cell Stem Cell 2015;17:35–46. 10.1016/j.stem.2015.05.003. [PubMed: 26095048]
52. Bowers E, Slaughter A, Frenette PS, Kuick R, Pello OM, Lucas D. Granulocyte-derived TNFa promotes vascular and hematopoietic regeneration in the bone marrow. Nat Med 2018;24:95–102. 10.1038/nm.4448. [PubMed: 29155425]
53. Passegué E, Jochum W, Schorpp-Kistner M, Möhle-Steinlein U, Wagner EF. Chronic myeloid leukemia with increased granulocyte progenitors in mice lacking junB expression in the myeloid lineage. Cell 2001;104:21–32. 10.1016/s0092-8674(01)00188-x. [PubMed: 11163237]
54. Ramalingam P, Poulos MG, Lazzari E, et al. Chronic activation of endothelial MAPK disrupts hematopoiesis via NFκB dependent inflammatory stress reversible by SCGF. Nat Commun 2020;11:666. 10.1038/s41467-020-14478-8. [PubMed: 32015345]

55. Pietras EM, Mirantes-Barbeito C, Fong S, et al. Chronic interleukin-1 exposure drives haematopoietic stem cells towards precocious myeloid differentiation at the expense of self-renewal. Nat Cell Biol 2016;18:607–18. 10.1038/ncb3346. [PubMed: 27111842]

HIGHLIGHTS

- Jak2 V617F and Ikk2-CA showed distinct and partly opposed effects on hematopoiesis.
- Jak2V617FandIkk2-CAbothantagonizedfrequencyoftrans-plantablehematopoieticstemcells(HSCs).
- Ikk2 transcriptionally altered thrombopoietin signalling to favour Stat1 over Stat3 activation.
- Double mutant gene expression suggested mutual antagonism in HSC but not GMP.
- Ikk2 and Jak2/Ikk2 mutant HSC showed a propensity toward apoptosis ex vivo.

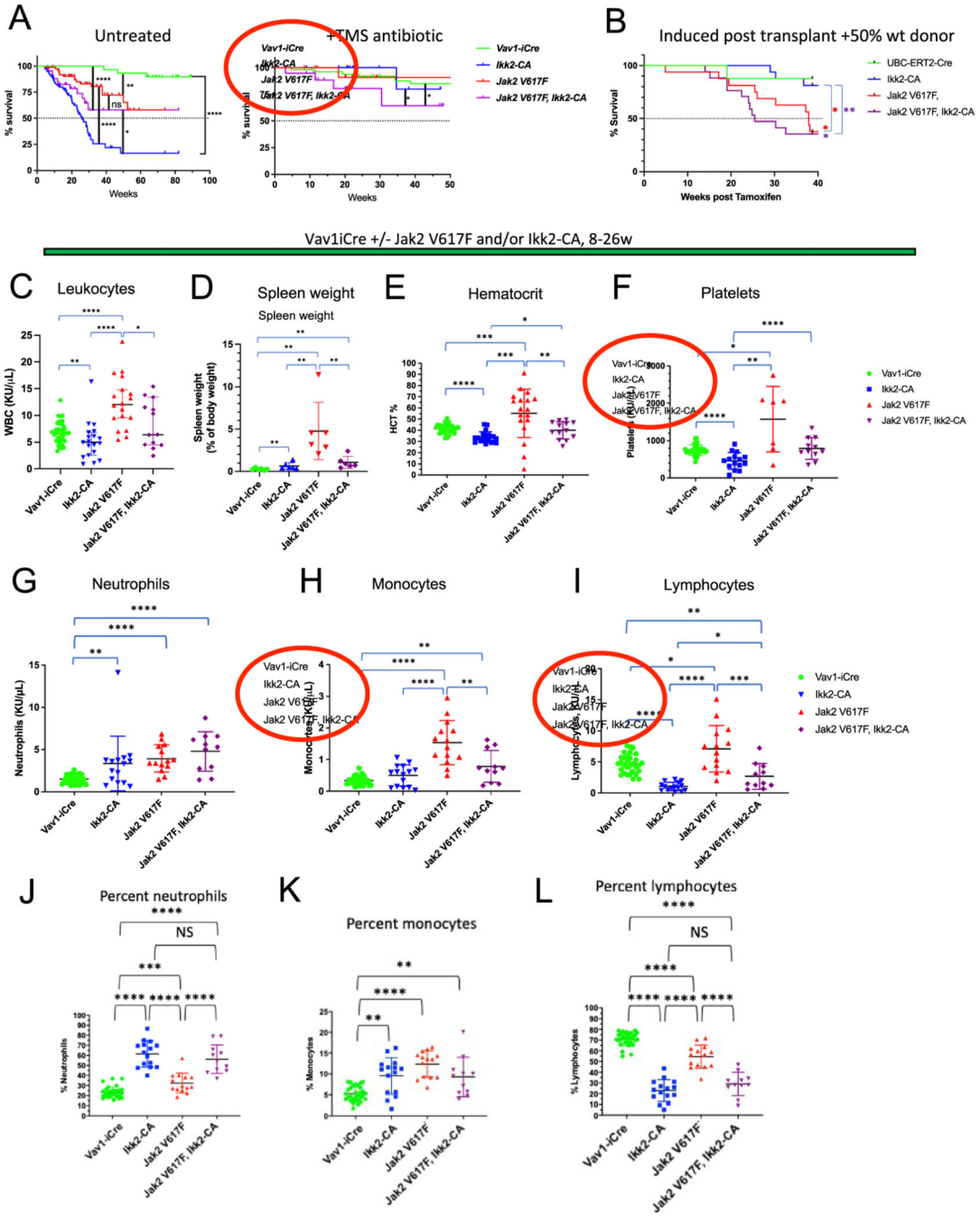

Figure 1.

Survival and blood parameters of Jak2 V617F, Ikk2-CA, and double mutant mice. **(A)** Survival curves of control Vav1-iCre, Ikk2-CA, Jak2 V617F, and double mutant mice up to >50 weeks postnatal, without (left) and with (right) antibiotics (trimethoprim, sulfamethoxazole) supplied in antibiotic water after weaning at 3−4 weeks postnatal. Bars between curves denote significance of differences between each pair of genotypes. Significance was determined by log-rank (Mantel−Cox) test. **(B)** Survival of transplant recipient mice in competitive transplant with tamoxifen induction of UBC-ERT2-Cre−driven

Jak2 V617F, Ikk2-CA, and double mutant genotypes (or UBC-ERT2-Cre alone as control), transplanted at 1:1 ratio with Cd45.1+ wild-type competitor, into lethally irradiated Cd45.1+ recipient mice. Significance as in **(A)**. **(C–F)** Blood parameters and spleen weight (D) for control Vav1-iCre, Ikk2-CA, Jak2 V617F, and double mutant mice, 8−26 weeks postnatal. **(C)** White blood cells (WBC). **(D)** Spleen weight. **(E)** Hematocrit. **(F)** Platelets. Error bars = mean ± 95% CI. **(G–I)** Absolute counts of neutrophils **(G)**, monocytes **(H),** and lymphocytes **(I)**. **(J–L)** Percentages of cells represented by neutrophils **(J)**, monocytes **(K)**, and lymphocytes **(L)**. Significance in **C−L** was determined by Mann-Whitney *U* test. In all graphs: *, $p < 0.05$, **, $p < 0.01$, ***, $p < 0.001$, ****, $p < 0.0001$.

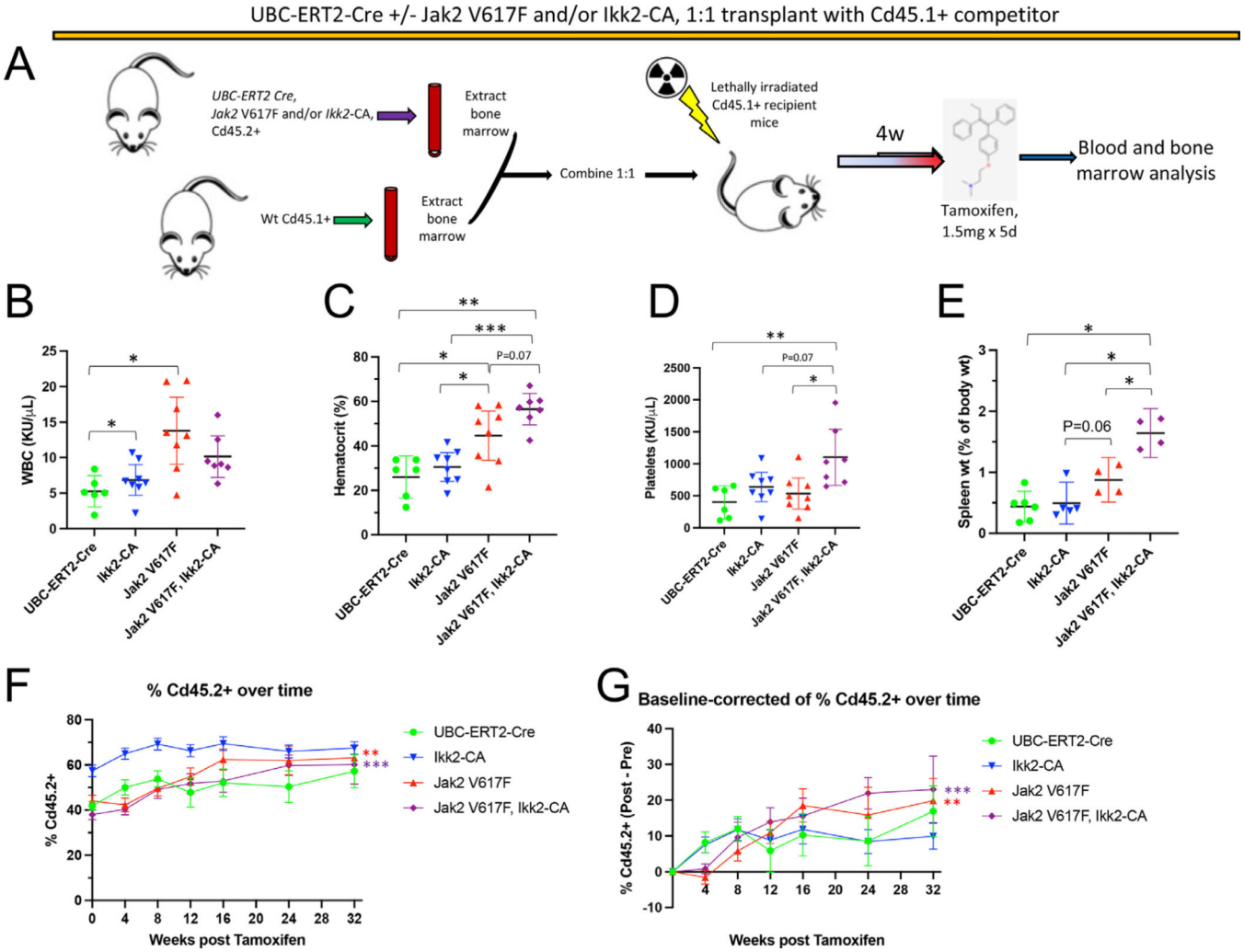

Figure 2.

Jak2 V617F, Ikk2-CA, and double mutant phenotypes in chimeric mice. **(A)** Schematic of competitive transplant and induction of UBC-ERT2-Cre−driven Jak2 V617F, Ikk2-CA, and double mutant chimeric mice. **(B–E)** Blood parameters for competitive transplant recipient mice, 12 weeks after induction with tamoxifen. **(B)** White blood cells (WBC). **(C)** Hematocrit. **(D)** Platelets. **(E)** Spleen weight of mice surviving mice sacrificed at 35 weeks posttamoxifen induction. Error bars = mean ± 95% CI. Significance in **(B−E)** was determined by Mann-Whitney *U* test: *, $p < 0.05$, **, $p < 0.01$, ***, $p < 0.001$, ****, $p < 0.0001$. **(F–G)** Absolute **(F)** and baseline-corrected **(G)** percentage of Cd45.2+ cells in the blood of competitive transplant recipients over 32 weeks following induction with tamoxifen. Significance (final vs. initial values) determined by two-tailed *t* test.

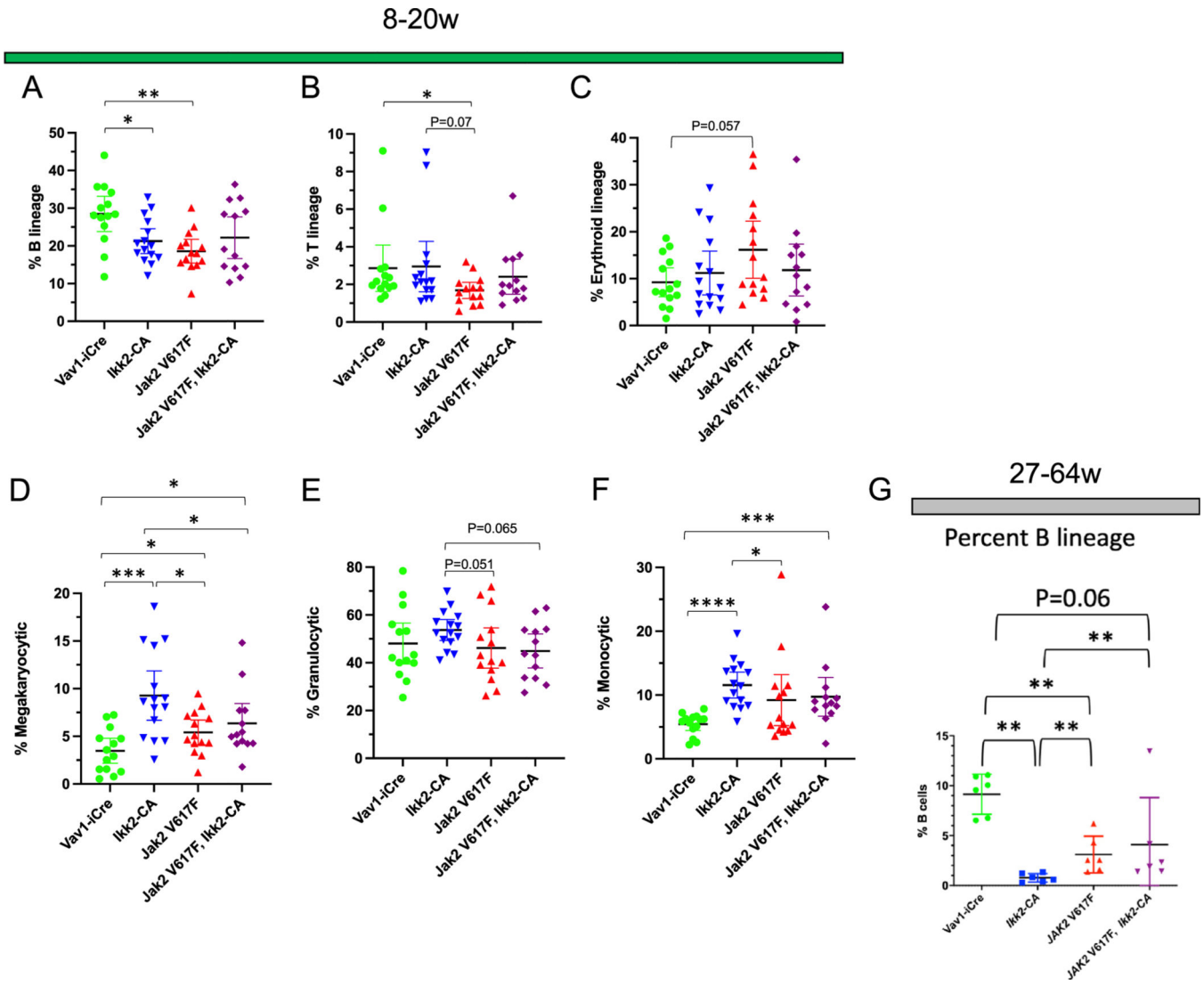

Figure 3.

Lineage differentiation in bone marrows of mutant mice. **(A–F)** Frequencies of differentiating lineages in bone marrows derived from 8- to 20-week-old control Vav1-iCre, Ikk2-CA, Jak2 V617F, and double mutant mice. **(A)** Percent B-cell lineage. **(B)** T-cell lineage. **(C)** Erythroid lineage. **(D)** Megakaryocytic lineage. **(E)** Granulocytic lineage. **(F)** Monocytic lineage. **(G)** Percent B-cell lineage in 27−64 weeks old control Vav1-iCre, Ikk2-CA, Jak2 V617F, and double mutant mice, showing depletion of B-cell lineage in older Ikk2-CA mice. Error bars = mean ± 95% CI. Significance was determined by Mann-Whitney *U* test: *, $p < 0.05$, **, $p < 0.01$, ***, $p < 0.001$, ****, $p < 0.0001$.

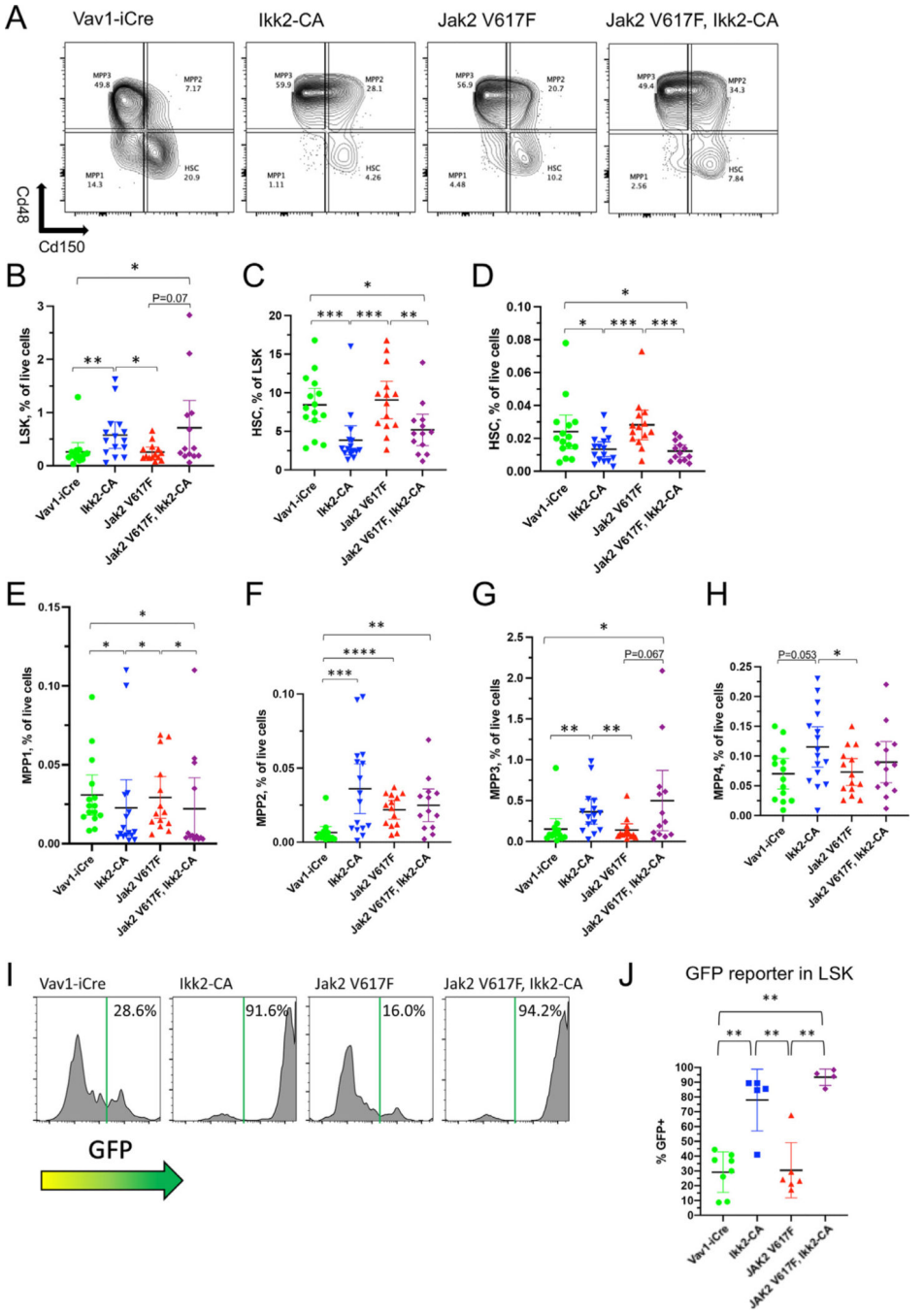

Figure 4.

Effects of *Jak2 V617F* and *Ikk2-CA* on HSC and MPP population frequencies. **(A)** Contour plots of LSKFlt3— population with from bone marrow of 8−12 weeks old Vav1-iCre control, Jak2 V617F, Ikk2-CA, and double mutant mice: Cd48 on y-axis and Cd150 on the x-axis provide quadrant gating into HSC, MPP1, MPP2, and MPP3 populations (these plots are also shown as Supplementary Figure E3D, along with gating for deriving parent population). **(B−H)** Graphs showing population frequencies in bone marrows of 8−20 weeks old mice: **(B)** LSK as percent of total live cells. **(C)** HSC as percent of LSK. **(D)** HSC as

percent of total live cells. **(E)** MPP1 as percent of total live cells. **(F)** MPP2 as percent of total live cells. **(G)** MPP3 as percent of total live cells. **(H)** Flt3+ MPP4 as a percentage of total live cells. **(I)** NFκB-induced GFP reporter in LSK from 8- to 12-week-old mice, with percentage of GFP+ cells indicated. (J) Quantification of percentage of GFP-positive LSK. Significance in **(B−H)** and **(J)** was determined by Mann-Whitney *U* test: *, $p < 0.05$, **, $p < 0.01$, ***, $p < 0.001$, ****, $p < 0.0001$. All error bars = mean ± 95% CI.

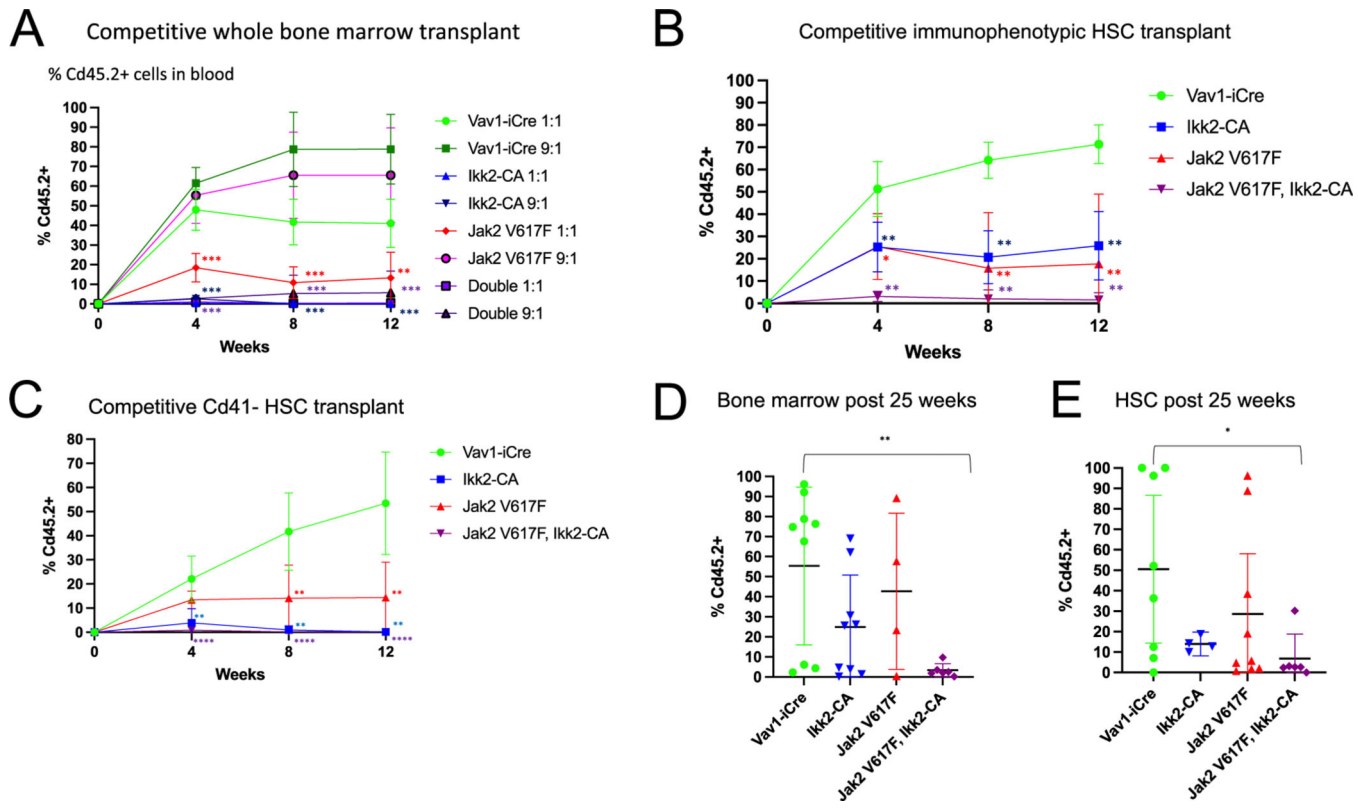

Figure 5.

Depletion of functional HSC in mutant genotypes. **(A)** Competitive whole bone marrow transplant. Whole bone marrow cells from Vav1-iCre control, Jak2 V617F, Ikk2-CA, and double mutant mice were transplanted in 1:1 and 9:1 ratios vs. Cd45.1 competitor bone marrow, with percent Cd45.2+ assessed in blood cells for 12 weeks after transplant. Error bars = mean ± SD. Significance is shown for 1:1 mutant transplants vs. Vav1-iCre control transplant. **(B)** Competitive immunophenotypic hematopoietic stem cell (HSC) transplant. 250 sorted HSCs from donor mice were transplanted together with 350,000 Cd45.1 whole bone marrow cells, with blood chimerism assessed for 12 weeks after transplant. **(C)** Competitive Cd41-transplant. 200 sorted Cd41-HSCs from donor mice were transplanted together with 350,000 Cd45.1 whole bone marrow cells, with blood chimerism assessed for 12 weeks after transplant. **(D)** Bone marrow of mice from A and B sacrificed at 25 weeks posttransplant: percent Cd45.2+ cells in total bone marrow. **(E)** Percent Cd45.2+ among bone marrow HSC, gated as in Supplementary Figure E8. Error bars in **(B–D)** = mean ± 95%CI, with significance determined of mutant chimerism vs. control. Significance in all graphs was determined by Mann-Whitney *U* test: *, $p < 0.05$, **, $p < 0.01$, ***, $p < 0.001$, ****, $p < 0.0001$.

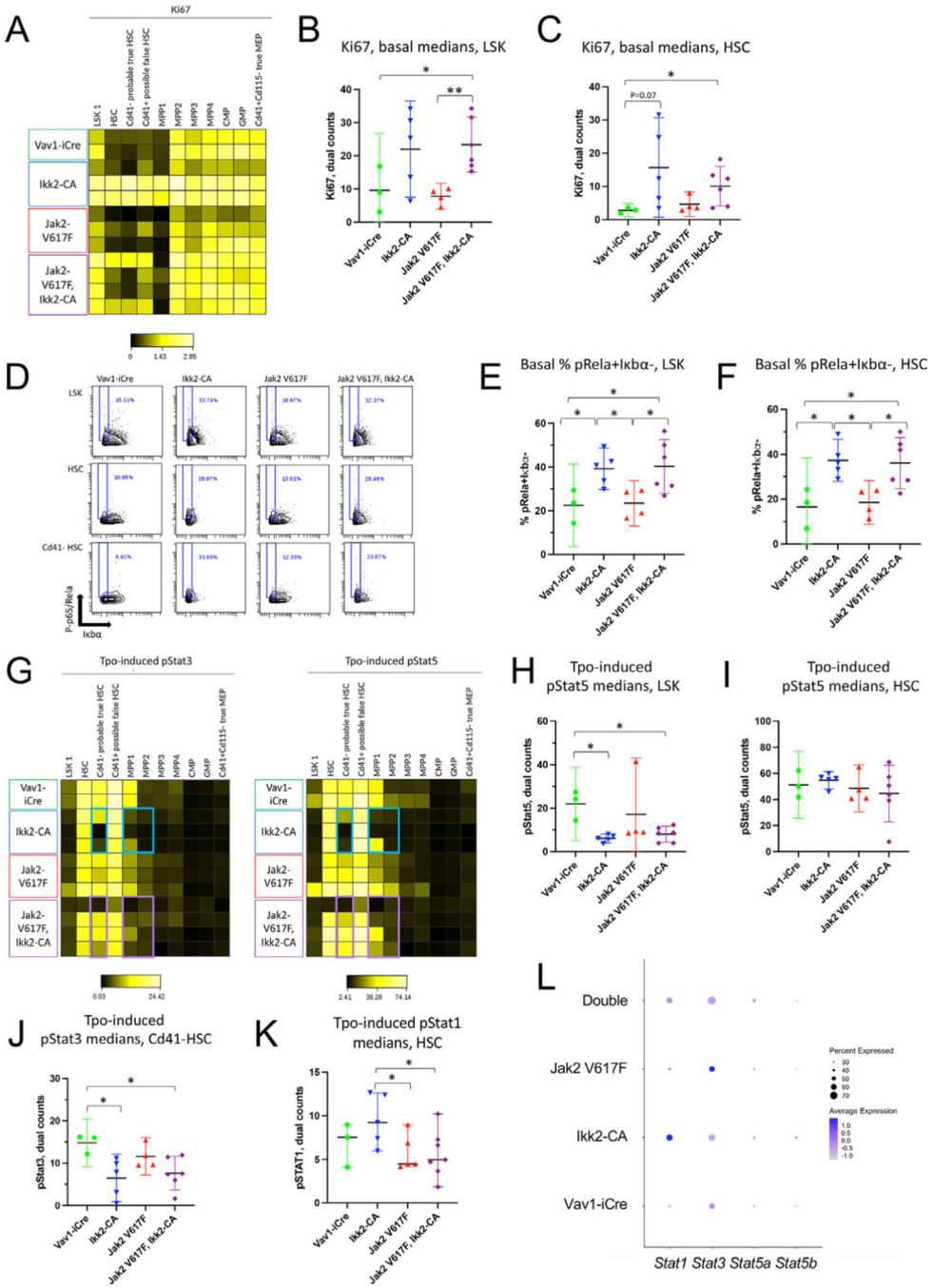

Figure 6.

Mass cytometry identification of Ikk2-CA effects on STATs. **(A)** Heat map showing median levels of Ki67 in HSPC populations measured in dual counts on the CyTOF2 mass cytometer, in absence of ex vivo stimulation. This experiment included two Vav1-iCre control mice, three each of Ikk2-CA and Jak2 V617F mice, and 4 double mutant mice, age 15−20 weeks postnatal. **(B)** Column graph of basal (unstimulated) Ki67 medians in total LSK population, combined from two experiments of the type shown in **(A). (C)** Column graph of basal (unstimulated) Ki67 medians in immunophenotypic HSC, from same

experiments as **(A)** and **(B). (D)** Contour plots showing levels of pRela (S536, y-axis) and total IκBα (x-axis), in (top to bottom rows) LSK, HSC, and Cd41-HSC populations. Gate is shown with percent of cells identified as pRela+ IκBα-in each cell population and genotype, in absence of ex vivo stimulation. **(E, F)** Column graph of percent of cells in pRela+ IκBα-gate (as in **D**) for LSK (**E**) and HSC **(F). (G)** Heat maps showing median levels of pStat3 (left) and pStat5 (right) in HSPC cell populations stimulated ex vivo with 25 ng/mL Tpo. Colored boxes denote cell populations in which median levels of pStat3 and pStat5 are reduced in some or all mutant mice (blue box, Ikk2-CA; violet box, double mutant) compared with controls. Scale indicates absolute signal levels in dual counts. **(H, I)** Column graphs showing median levels of pStat5 in LSK **(H)** and HSC **(I). (J)** Column graph of median pStat3 levels in Cd41-HSC. **(K)** Column graph of median pStat1 levels in Tpo-stimulated HSC. Error bars in **(B, C, E, F, H–K)** = mean ± 95% CI. Significance was determined by Mann-Whitney *U* test: *, $p < 0.05$, **, $p < 0.01$, ***, $p<0.001$. **(L)** Dot plot of mRNA detection from single cell RNA sequencing in HSC+MPP population (Figure 6) in each genotype, for expression of Stat1, Stat3, Stat5a, and Stat5b. Circle size scale indicates percent of cells in which the transcript was detected. Color intensity indicates relative transcript level below maximum (= 1) on Log(2) scale.

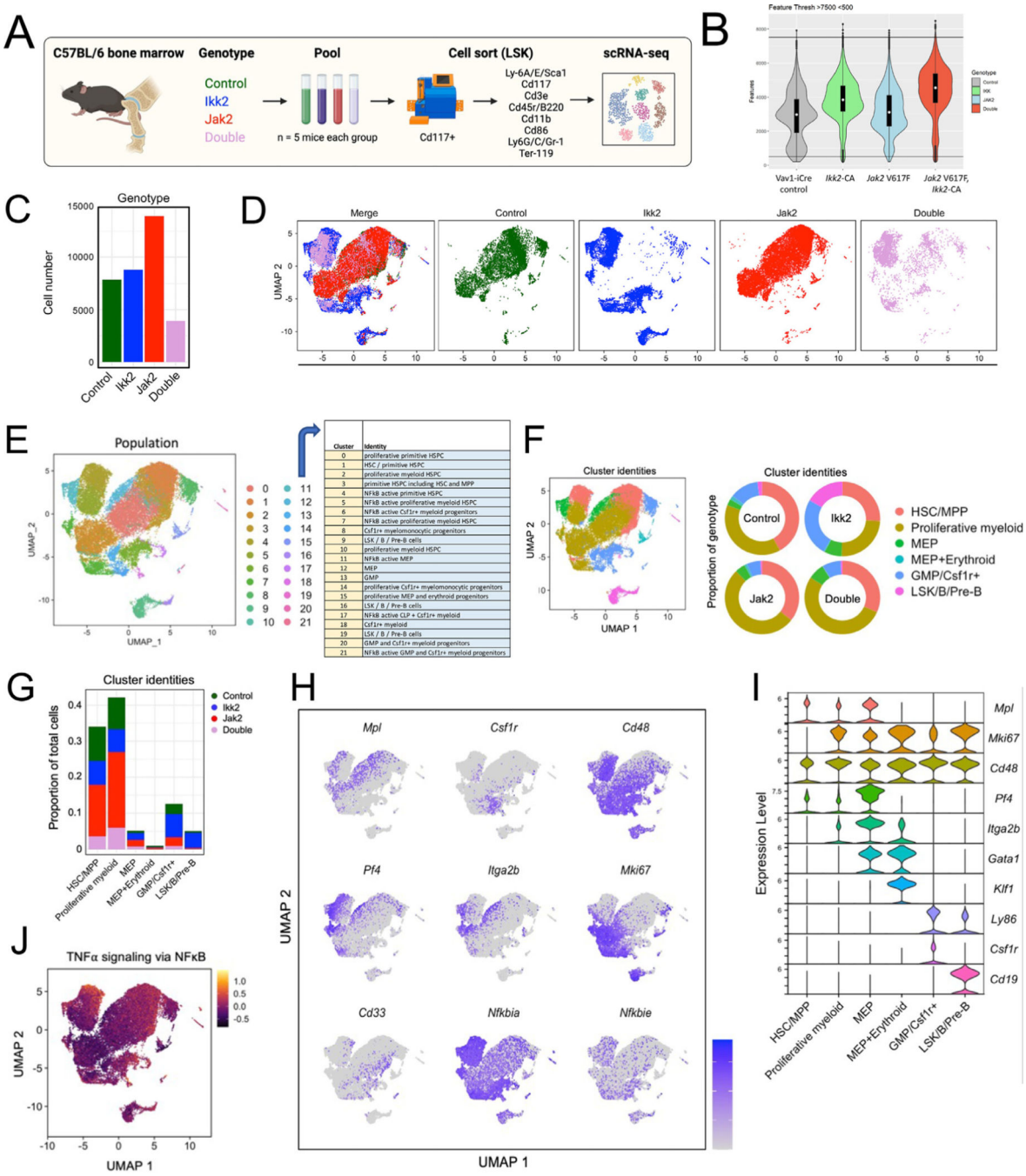

Figure 7.

Single-cell RNA sequencing of bone marrow LSK cells. **(A)** Schematic of cell collection procedure for LSK (Lin-Kit+Sca-1+). **(B)** Graph showing features (transcripts of unique genes) per cell from Cell Ranger, with capture quality cutoffs of 500<(features) <7,500. **(C)** Cell number obtained per sample in Seurat, after cutoffs for features **(B)** and <9% mitochondrial transcripts per cell. **(D)** Seurat UMAP with contributions of individual genotypes. **(E)** Cell clusters generated by Seurat unanchored clustering. **(F, G)** Cell population identities as determined from differential gene expression of cell

clusters, with proportions of populations in each genotype **(F)** and of each genotype within each grouped cell population **(G). (H)** UMAPs showing expression of examples of individual genes used for cluster identification: canonical HSPC cell population markers *Mpl, Csf1r, Cd48, Pf4, Itga2b*, and *Cd33*; proliferation marker *Mki67*, and NF*κ*B target genes *NFκBia* and *NFκBie*. **(I)** Violin plots showing gene expression of canonical markers of hematopoietic cell populations, used to define cluster populations in **(E−G). (J)** Color intensity labeled UMAP showing graded expression of the gene set HALLMARK_TNFA_SIGNALING_VIA_NF*κ*B. Expression intensity is highest in areas expressing *NFκBia* but negative for *Mki67* (compare with **H**), in HSC+MPP and *Csf1r*+/GMP cell groups (compare with **F**) but not exclusive to the distribution of any individual genotype(s) (compare with **D**).

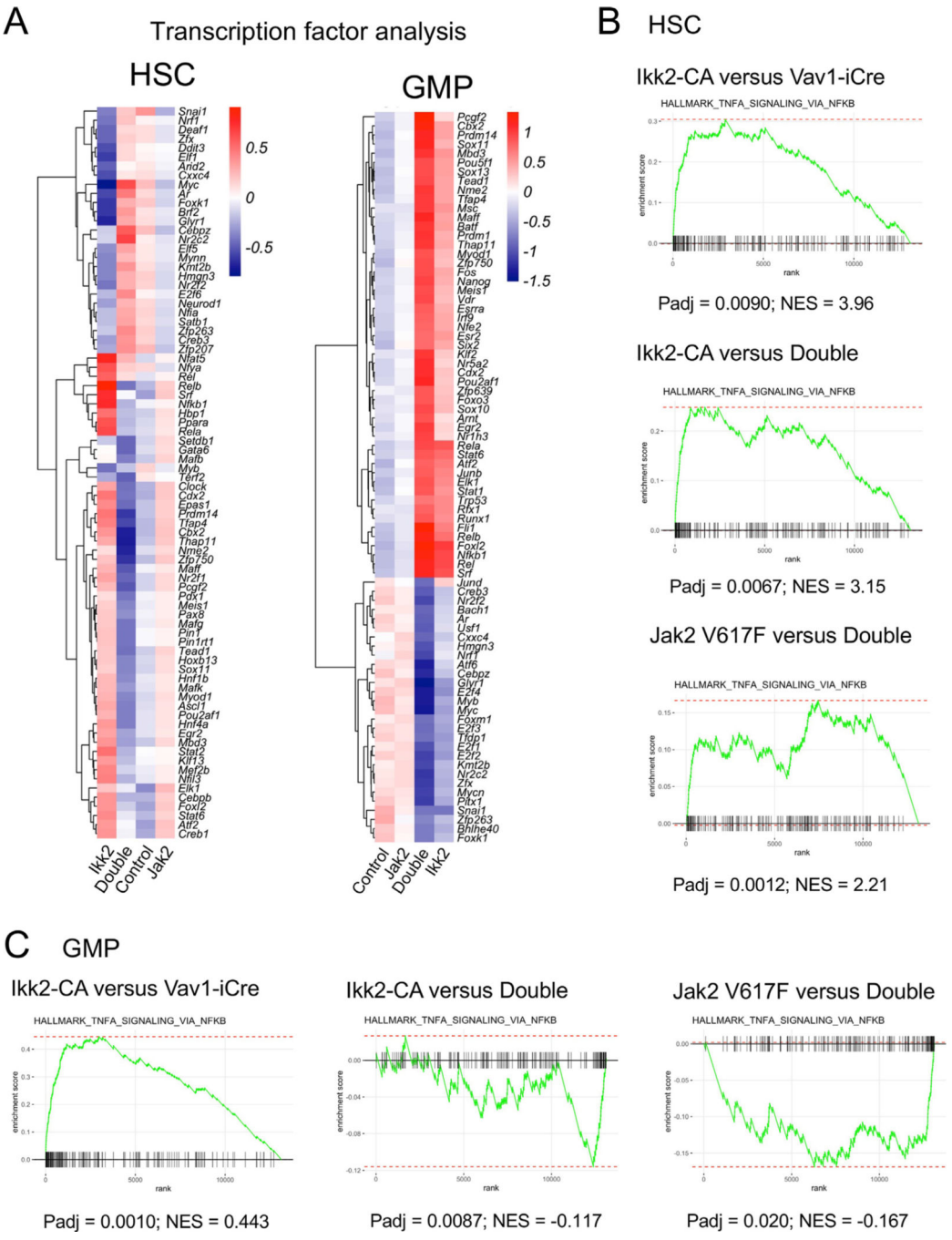

Figure 8.

Distinct transcriptional interactions of Jak2 and Ikk2 in HSC vs. GMP. **(A)** Transcription factor gene expression heatmaps for HSC (clusters 1+3, left) and GMP (clusters 13+20+21, right). **(B, C).** Gene enrichment plots for gene set HALLMARK_TNFA_SIGNALING_VIA_NFKB in HSC **(B)** and GMP **(C)**, with comparisons, right to left, of Ikk2-CA vs. Vav1-iCre control; Ikk2-CA vs. double mutant; Jak2 V617F vs. double mutant.

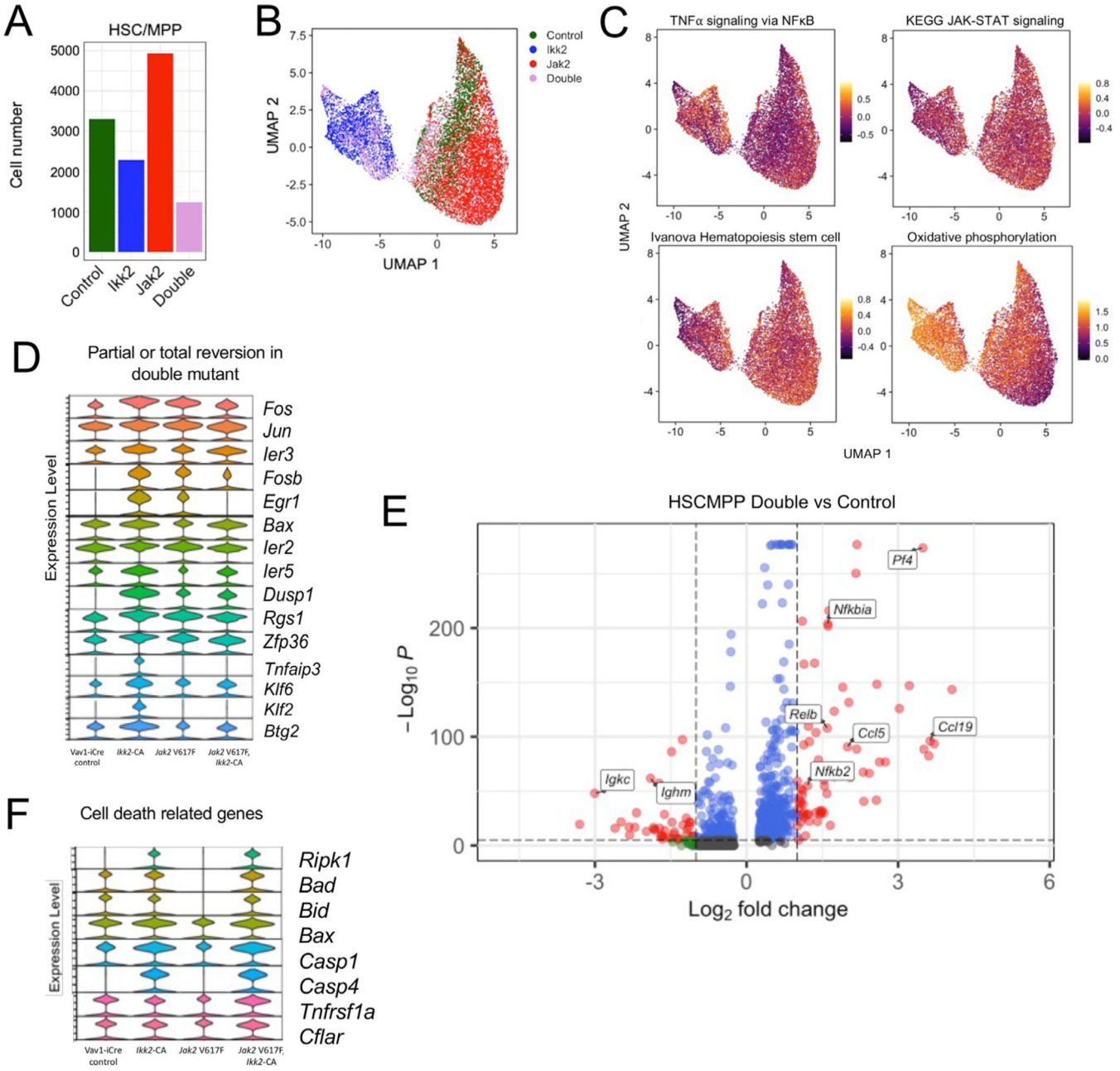

Figure 9.

Differential gene expression in HSC and MPP. **(A)** Graph of cell number for each genotype in HSC+MPP population (clusters 1+3+4, Figure 4E). **(B)** UMAP of HSC+MPP population labeled in color for each genotype. **(C)** UMAP of HSC+MPP population colored for expression of differentially expressed gene sets. Above, HALLMARK_TNFA_SIGNALING_VIA_NFκB (left) and KEGG_JAK-STAT_SIGNALING (right). Below, IVANOVA_HEMATOPOIESIS_STEM_CELL (left) and OXIDATIVE_PHOSPHORYLATION (right). **(D)** Violin plots of selected genes upregulated in both single mutants vs. control but downregulated in double mutant vs.

both single mutants. **(E)** Volcano plot of differentially expressed genes in double mutant vs. control. **(F)** Violin plots of selected genes related to cell death.

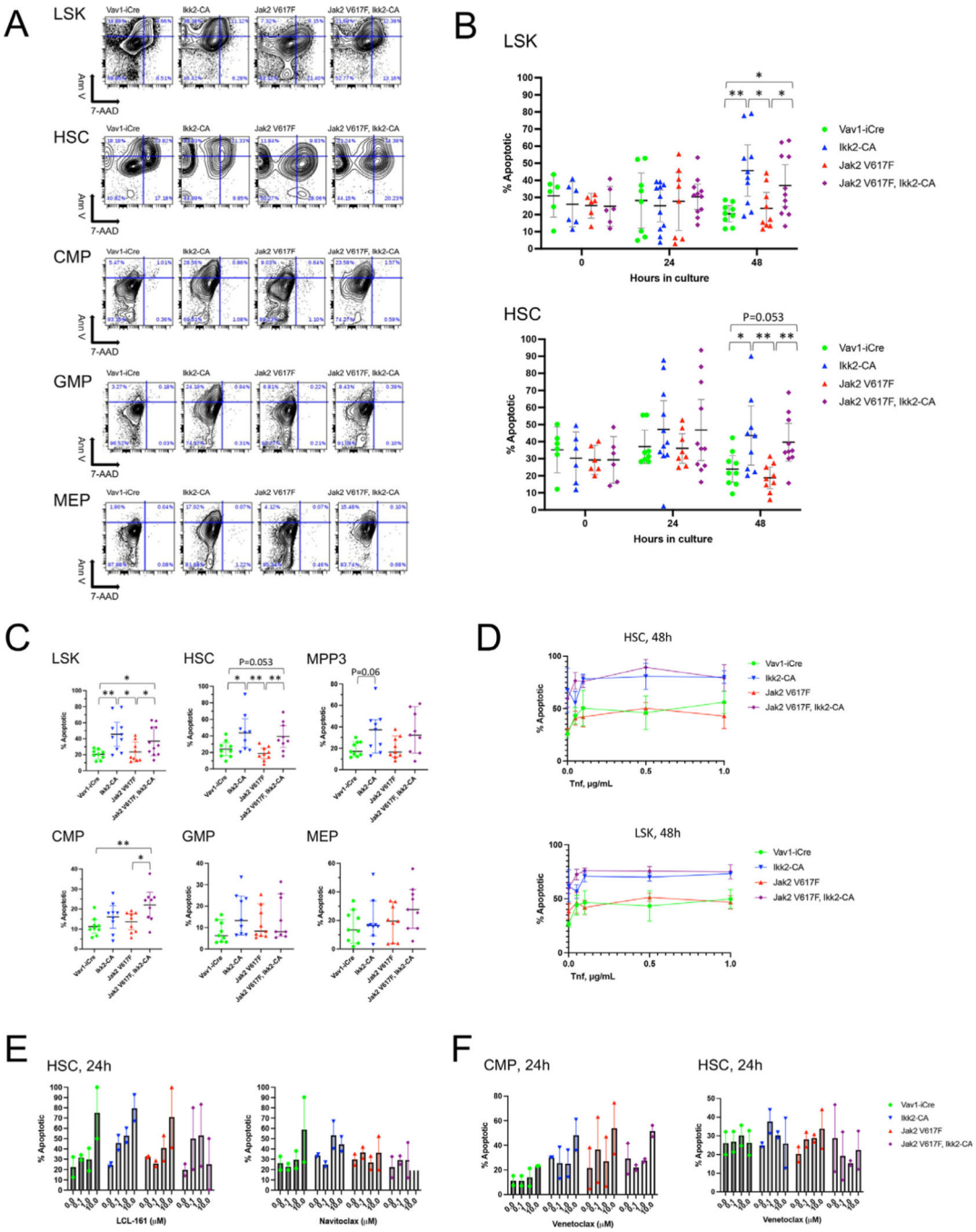

Figure 10.

Ikk2-CA dominantly enhances apoptotic vulnerability of HSC ex vivo. Results of apoptosis assay, 48 hours ex vivo. **(A)** Biaxial contour plots with apoptotic marker Annexin V (Ann V, y-axis) vs. cell death label 7-AAD (x-axis). Each plot shows cells from an individual mouse in the experiment. Genotypes, left to right columns: Vav1-iCre, Ikk2-CA, Jak2 V617F, and double mutant. Rows, top to bottom: LSK, HSC, MPP3, CMP, GMP, MEP. **(B)** Progression of Annexin V+ apoptotic cells over time in culture for total LSK (left) and HSC (right). Error bars = mean ± 95%CI. **(C)** Graphs of percent apoptotic cells post 48h ex vivo. Graphs,

as labeled, of LSK, HSC, CMP, GMP, and MEP. Error bars = mean ± 95%CI. Significance was determined by Mann-Whitney U test: *, $p < 0.05$, **, $p < 0.01$. **(D)** Dose−response graphs of Annexin V positive cells in response to Tnf in 48-hour culture, for HSC (above) and total LSK (below). Error bars = mean ± SD. $N = 3$ individual mice from each genotype. **(E)** Dose−response showing percent of apoptotic cells among HSC treated in 24-hour ex vivo culture with LCL-161 (left) and navitoclax (right). **(F)** Dose−response of apoptotic cells among CMP (left) and HSC (right) treated in 24-hour ex vivo culture with venetoclax. Error bars in **(E, F)** = mean plus range of two separate experiments, each using pooled Kit+ cells from three mice of each genotype.